Research Paper

GEOSPHERE

GEOSPHERE, v. 18, no. 4

https://doi.org/10.1130/GES02434.1

13 figures; 4 tables; 1 set of supplemental files

CORRESPONDENCE: lon.abbott@colorado.edu

CITATION: Abbott, L.D., Flowers, R.M., Metcalf, J., Falkowski, S., and Niazy, F., 2022, Post-Laramide, Eocene epeirogeny in central Colorado—The result of a mantle drip?: Geosphere, v. 18, no. 4, p. 1223–1246, https://doi.org/10.1130/GES02434.1.

Science Editor: Andrea Hampel
Associate Editor: Gregory D. Hoke

Received 15 March 2021
Revision received 23 November 2021
Accepted 16 February 2022

Published online 12 May 2022

Post-Laramide, Eocene epeirogeny in central Colorado—The result of a mantle drip?

Lon D. Abbott[1], Rebecca M. Flowers[1], James Metcalf[1], Sarah Falkowski[2], and Fatima Niazy[3,4]

[1]Department of Geological Sciences, University of Colorado Boulder, 399 UCB, Boulder, Colorado 80309, USA
[2]Department of Geosciences, University of Tübingen, Schnarrenbergstr. 94-96, 72076 Tübingen, Germany
[3]Department of Earth and Ocean Sciences, Tufts University, Lane Hall, Medford, Massachusetts 02155, USA
[4]Research Experiences in Solid Earth Science for Students (RESESS), UNAVCO, 5350 Nautilus Drive Suite B/C, Boulder, Colorado 80301-5394, USA

ABSTRACT

The Southern Rocky Mountains first rose during the Laramide Orogeny (ca. 75–45 Ma), but today's mountains and adjacent Great Plains owe their current height to later epeirogenic surface uplift. When and why epeirogeny affected the region are controversial. Sedimentation histories in two central Colorado basins, the South Park–High Park and Denver basins, shifted at 56–54 Ma from an orogenic to an epeirogenic pattern, suggesting central Colorado experienced epeirogeny at that time. To interrogate that hypothesis, we analyzed thermal histories for seven samples from central Colorado's Arkansas Hills and High Park using thermochronometers with closure temperatures below ~180 °C, enabling us to track sample exhumation from ~5–7 km depth.

Three samples are from the Cretaceous Whitehorn pluton, and four are Precambrian granitoids. All zircon and titanite (U-Th)/He dates (ZHe and THe) and one apatite fission-track (AFT) date are similar to the 67 Ma pluton emplacement age. Whitehorn dates using the lower-temperature apatite (U-Th)/He (AHe) thermochronometer are 55–41 Ma. These data require two exhumation episodes, one ca. 67–60 Ma, the second beginning at 54–46 Ma. The pluton reached the surface by 37 Ma, based on the age of volcanic tuff filling a pluton-cutting paleovalley. The Precambrian samples do not further refine this thermal history owing to the comparatively higher He closure temperature of their more radiation-damaged apatite.

Laramide crustal shortening caused 67–60 Ma exhumation. Arkansas Hills shortening ended before 67 Ma, so shortening could not have caused the exhumation event that began 54–46 Ma; thermochronology supports the Eocene epeirogeny hypothesis. Epeirogeny affected >2.0 × 10^4 km^2, from the Sawatch Range to the Denver Basin. We attribute epeirogeny to an Eocene mantle drip that likely triggered subsequent drips, causing younger exhumation events in adjacent areas.

Lon Abbott https://orcid.org/0000-0002-6353-0645

INTRODUCTION

Today's Southern Rocky Mountains (SRM) consist of multiple discrete ranges and flanking synorogenic basins (Fig. 1) that were produced by crustal shortening during the Laramide orogeny (ca. 75–45 Ma; Tweto, 1975; Dickinson et al., 1988). Although the modern mountains are built on this orogenic foundation, broad consensus exists that the SRM achieved the current surface elevation (sensu England and Molnar, 1990) of ~2.8 km due to *epeirogenic* uplift (e.g., Trimble, 1980; Bird, 1988; Eaton, 2008; Cather et al., 2012; Karlstrom et al., 2012).

Consensus evaporates when questions turn to *when* and *why* the SRM and adjacent Great Plains experienced epeirogenic uplift. Modern SRM ranges are exhumed facsimiles of their Laramide predecessors. Post-Laramide deposition switched to erosion ca. 5 Ma, stripping easily eroded sediment from the resistant, previously buried crystalline cores to re-expose the Laramide ranges. Many workers thus conclude epeirogeny occurred ca. 5 Ma (e.g., Epis and Chapin, 1975; Trimble, 1980; Karlstrom et al., 2012). Others argue global cooling at 5 Ma caused the switch to erosion; they favor earlier epeirogeny (e.g., Molnar and England, 1990; Gregory and Chase, 1992; Pelletier, 2009). Some workers suggest an Eocene or Oligocene start to a still active epeirogeny (e.g., Sahagian et al., 2002; Eaton, 2008). Others invoke multiple epeirogenic episodes with different causes (e.g., Cather et al., 2012; Karlstrom et al., 2012). This surfeit of hypotheses highlights the need to constrain the timing of post-Laramide surface uplift event(s) to preclude some mechanisms and elevate others to a short list of likely candidates.

We present new low-temperature thermochronology for central Colorado's Arkansas Hills that documents Eocene exhumation beginning between 54 and 46 Ma, long after Laramide crustal shortening had ended. Next, we examine the sedimentary histories of the South Park–High Park and Denver basins (Fig. 1), showing that Arkansas Hills exhumation was coeval with formation of basin unconformities that mark the end of subsidence there. We interpret these coeval events to record Eocene epeirogenic surface uplift in central Colorado. Lastly, we explore published mechanisms to explain the epeirogeny and suggest a new one—foundering of a lithospheric drip.

THE LARAMIDE OROGENY: ITS TIMING AND CAUSE

We distinguish here between epeirogenic and orogenic surface uplift, so we must establish the temporal, spatial, and process connotations of our use of the term "Laramide orogeny," a term that has been ascribed multiple meanings. Here we follow Tweto (1975) and DeCelles (2004), defining

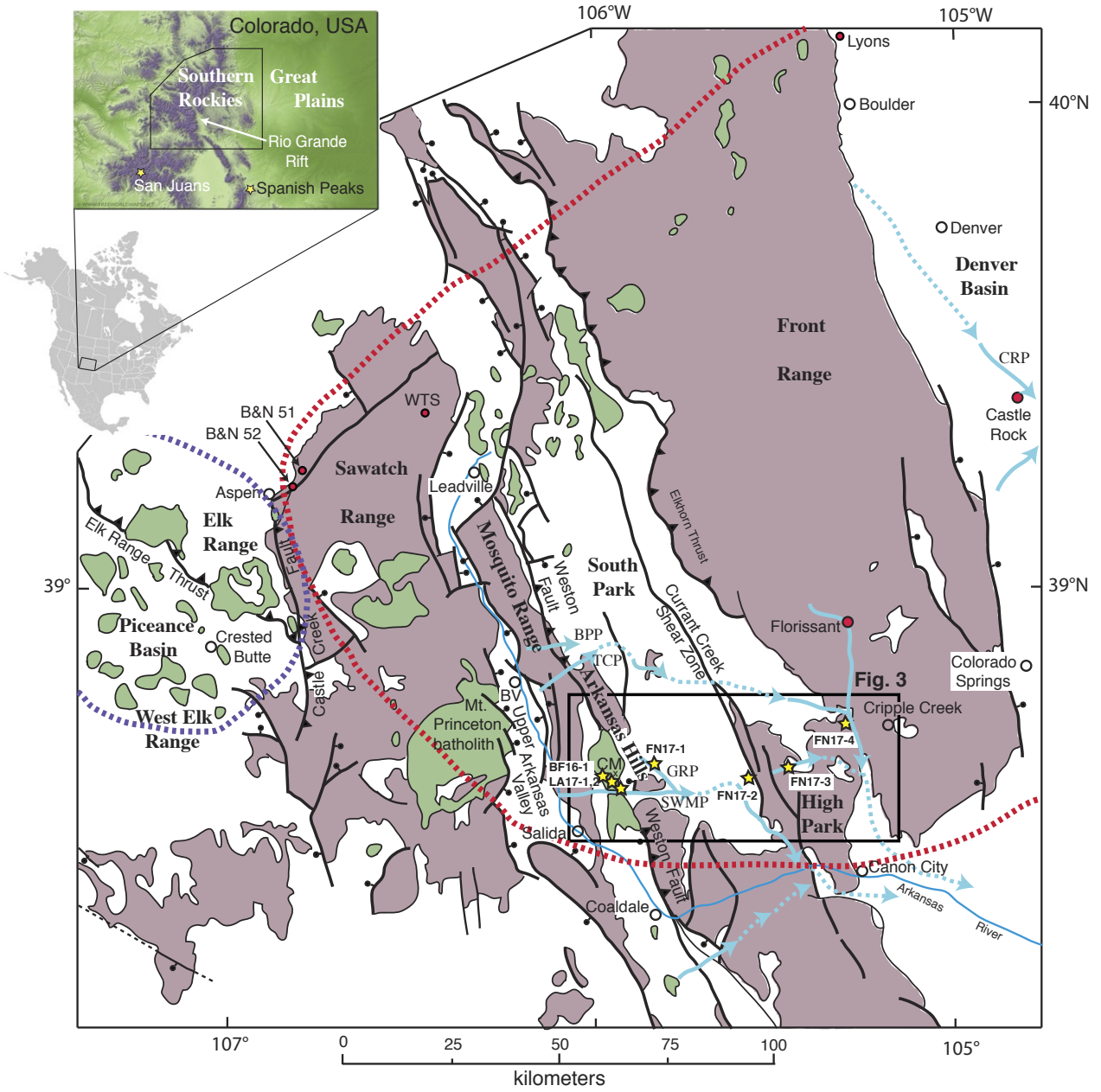

Figure 1. Map of central Colorado, showing key features. The Laramide-age Sawatch anticline (active ca. 73–68 Ma) was later split by the Rio Grande Rift to form the Upper Arkansas Valley. Today's Elk, Sawatch, Mosquito and Arkansas Hills ranges comprise that Laramide-age anticline. The Laramide-age Front Range (active ca. 64–54 Ma) is intact. South Park and High Park together constitute the Laramide-age South Park–High Park Basin. Locations mentioned in the text that contain key evidence for epeirogeny are shown with red dots. The minimum area affected by the Eocene epeirogeny is surrounded by the red dashed line and the Gothic Dome is shown by the purple dashed line. Our thermochronology samples are marked with yellow stars. Eocene paleovalleys are marked with light blue arrows. SWMP—Salida-Waugh Mountain paleovalley; GRP—Gribbles Run paleovalley; TCP—Trout Creek paleovalley; BPP—Buffalo Peaks paleovalley; CRP—Castle Rock paleovalley; CM—Cameron mountain; BV—town of Buena Vista; WTS—West Tennessee Stock, B&N 51 and B&N 52 are the Bryant and Naeser (1980) 51 Ma and 52 Ma apatite fission-track samples, respectively. The area shown in Figure 3 is outlined. Features mentioned in the text are labeled. The inset map locates the figure in North America and Colorado and shows the spatial relationship of the Spanish Peaks, discussed in the text, to our study area. Modified from Bryant and Naeser (1980).

the Laramide orogeny as an episode of basement-involved reverse faulting in the Cordilleran foreland between Late Campanian and middle Eocene time.

Given this regional ca. 75–45 Ma timing for the Laramide orogeny, studies commonly label any rock uplift or exhumation event that transpired between 75 and 45 Ma as "Laramide" and ascribe its cause to crustal shortening. But the initiation and cessation of crustal shortening (i.e., orogenic mountain building) was diachronous across the Laramide province (e.g., Tweto, 1975; Copeland et al., 2017). A given SRM event that falls within the canonical "Laramide" time window may or may not have been caused by crustal shortening. Here we use the term "Laramide" to refer to a crustal shortening (i.e., orogenic) event or its timing in a specific SRM range. We classify any event that postdates crustal shortening in that range as "post-Laramide," even if it occurred during the 75–45 Ma time span of regional Laramide orogenic activity. As argued below, Laramide shortening ended in our Arkansas Hills study area by 67 Ma; any post–67 Ma event, including the epeirogenic surface uplift we infer, is therefore "post-Laramide."

GEOLOGIC BACKGROUND

Our study area, which stretches from the Arkansas Hills to High Park (Fig. 1), has experienced a complex geologic history. Here we recap that history, highlighting events of particular relevance for assessing the implications of our thermochronologic results (Table 1).

Pre-Laramide Events

Central Colorado's Proterozoic crystalline basement underlies a 300-m-thick early Paleozoic sedimentary sequence (Tweto, 1987). The Pennsylvanian–Permian-aged Ancestral Rockies orogeny then raised two highlands separated by a sedimentary basin—the Central Colorado Trough (Ye et al., 1996; Barkmann et al., 2016). Older sediments were stripped from the highlands while kilometers of synorogenic sediment accumulated in the Central Colorado Trough. The Arkansas Hills (Fig. 1; Table 1), which lay in the ancient basin, contain 3.4–5.8 km of Paleozoic sediment (Wofford, 1986). High Park lies in the ancient highlands, so Jurassic sediments unconformably overlie Precambrian basement (Figs. 2 and 3; Wobus et al., 1979).

Late Mesozoic Colorado was covered by the Western Interior Seaway (WIS), in which 1.5–3.0 km of sediment accumulated (Cross and Pilger, 1978), with 500–1600 m now exposed in the Arkansas Hills (Wofford, 1986). When the Laramide orogeny began, Arkansas Hills basement was mantled by 5–8 km of Phanerozoic sediment; whereas in High Park, the basement had only 0.5–1.5 km of sedimentary cover (Fig. 2; Table 1).

Laramide Orogeny: The Sawatch Anticline and the Whitehorn Granodiorite

The asymmetric Sawatch anticline rose early in the Laramide orogeny (Tweto, 1975) atop the Elk Range thrust and the Castle Creek reverse fault, both near Aspen (Fig. 1; Table 1; Bryant, 1966; Kellogg, 1999). It rose above sea level after 75 Ma based on Mancos Formation ammonite dates; faulting was active by 72–70 Ma (Tweto, 1975). Later rifting split the anticline (see Development of the Rio Grande Rift [RGR] section), separating the Arkansas Hills, its southeastern flank, from the Sawatch Range (Fig. 4A).

The Arkansas Hills consists primarily of east-dipping Paleozoic sediment overlying basement. The syn-Laramide Whitehorn Granodiorite cross-cuts the Weston fault (Fig. 3; Wrucke, 1974; Wrucke and Dings, 1979; Wallace et al., 2000), which is the dominant Laramide structure in the Hills. Thus, Arkansas Hills thrusting ended before Whitehorn intrusion. Abbey et al. (2017) obtained a 67 Ma zircon U/Pb date on the Whitehorn (67.31 +0.57/–0.78 Ma). Wofford (1986) constrained pluton emplacement to

TABLE 1. SUMMARY OF CENTRAL COLORADO GEOLOGIC HISTORY

Time period or event	Sawatch Anticline (Arkansas Hills)	South Park–High Park	Front Range	Denver Basin
Precambrian/early Paleozoic	Formation of the basement and deposition of a thin (~300 m) passive margin sedimentary pile.			
Ancestral Rockies orogeny	Part of the central Colorado Trough, 3.4–5.8 km of sediment accumulates.	Mostly part of the Ancestral Front Range Highland. No Paleozoic sediment accumulates.	Location of the Ancestral Front Range Highland. No Paleozoic sediment accumulates.	Receives sediment from the Ancestral Front Range.
Western Interior Seaway	Entire region covered by ocean. Subsidence allows accumulation of 1.5–3-km-thick sequence.			
Laramide orogeny	Rises early in the episode (ca. 74–67 Ma). No later active shortening.	Intermontane basin. South Park receives 2 km of synorogenic sediment (69–56 Ma).	Locus of shortening shifts to here from the Sawatch (ca. 69–54 Ma).	Foreland basin. Receives at least 900 m of synorogenic sediment (69–54 Ma).
Eocene–Oligocene	Exhuming between 52–46 Ma and 37 Ma. Ash flows fill paleochannels.	Unconformity 56–38 Ma forms Rocky Mountain Erosion Surface (RMES). Overlain by cut-and-fill sedimentary and/or volcanic fill.	RMES forms by late Eocene. Overlain by Wall Mountain Tuff and other ash flows.	Unconformity spanning 54–41 Ma. Cut-and-fill sedimentary and/or volcanic fill thereafter.

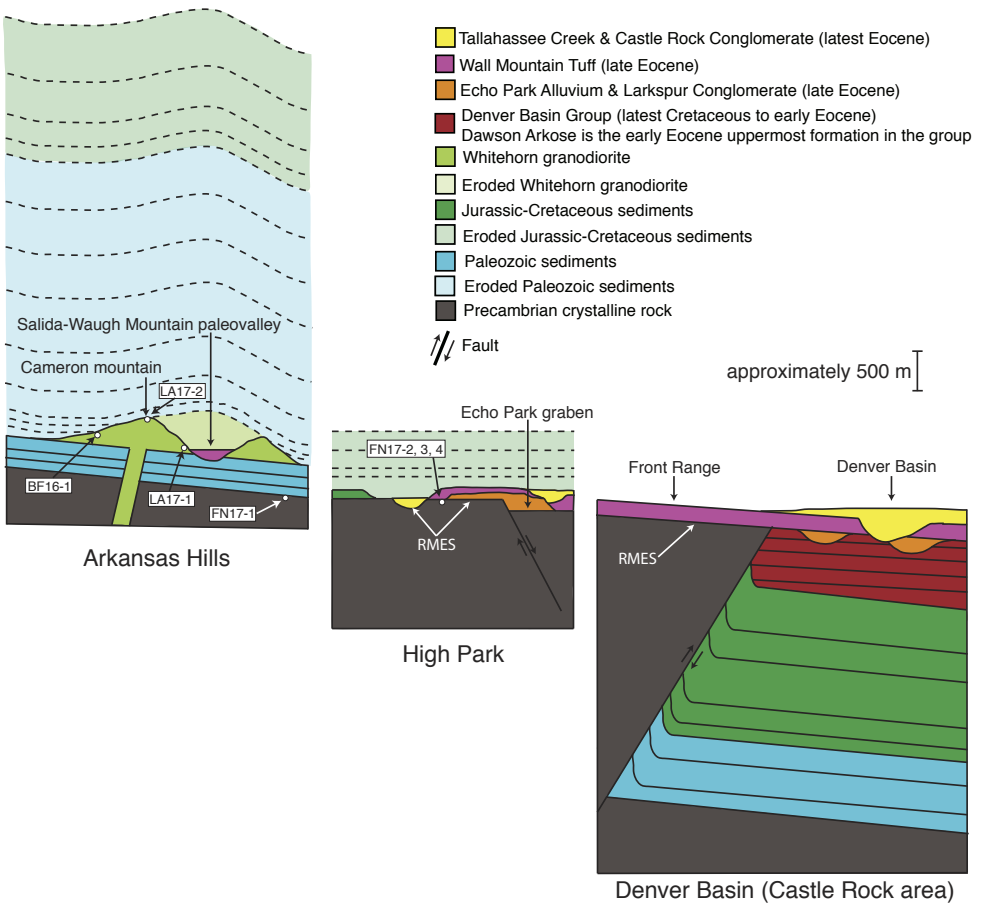

Figure 2. Schematic stratigraphic columns showing the stratigraphic relationships in the Arkansas Hills, High Park, and the Front Range–Denver Basin interface (Castle Rock). Note the cut-and-fill nature of the late Eocene units in the High Park and Denver basins. The greater magnitude of exhumation in the Arkansas Hills portion of the study area compared to the High Park area is shown, with eroded material shown with a more transparent color. RMES—Rocky Mountain Erosion Surface. See Figure 1 for the locations of each column.

3.0–7.5 km based on sediment thickness; Abbey et al. (2017) narrowed that to 5–7 km depth (see below). Farther north, in the Mosquito Range, fault activity continued into the early Paleocene (post–65–63 Ma; Bohannon and Ruleman, 2013).

Sedimentary histories in the Piceance Basin to the west (Obradovich, 1969; Foreman and Rasmussen, 2016) and South Park to the east (Fig. 1; Tweto, 1975; Barkmann et al., 2016) confirm a late Cretaceous–early Paleocene uplift age for the Sawatch anticline. Paleocurrents and provenance (i.e., Paleozoic clasts) in early synorogenic sediment of both basins have a Sawatch source. The 69 Ma base of the South Park Formation (South Park's synorogenic fill) rests unconformably atop progressively younger rocks farther east, revealing pre–69 Ma Sawatch uplift and erosion (Barkmann et al., 2016). Clast provenance and east-flowing paleocurrents continue to record a Sawatch source until 60 Ma, based on the 59.7 ± 2.0 Ma K/Ar date on a tuff just below an intraformational unconformity (Bryant et al., 1981; Barkmann et al., 2016).

The upper South Park Formation then records an eastward shift in the locus of shortening from the Sawatch to the Front Range. Paleocurrents reverse to a westward flow, sourced from the Front Range, above the unconformity. Paleozoic clasts disappear in the upper, arkosic, 60–56 Ma portion of the formation, replaced by clasts of Precambrian granite and gneiss (Barkmann et al., 2016) derived from the Front Range. The South Park Formation itself was then underthrust beneath Precambrian basement along the west-vergent Elkhorn Thrust during Laramide rise of the Front Range (Obradovich et al., 1969; Tweto, 1975; Raynolds, 1997; Barkmann et al., 2016).

To summarize, although the Laramide orogeny continued elsewhere in the Rockies until ca. 45 Ma, crustal shortening and concomitant rock uplift ceased in the southeastern Sawatch anticline, the location of our study area, by ca. 67 Ma (Table 1). Exhumation of the Sawatch highland in response to that crustal shortening had dwindled by 60 Ma.

Creation of the Rocky Mountain Erosion Surface, Paleovalleys, and the Ignimbrite Flare-Up

Extensive erosion in the aftermath of the Laramide orogeny planed off the Laramide Rockies to form the widespread, mostly low relief Rocky Mountain Erosion Surface (RMES) before 38 Ma (Fig. 2; e.g., Epis and Chapin, 1975; Scott, 1975; Colman, 1985; Scott and Taylor, 1986). We know the RMES in central Colorado had formed by the late Eocene because it is blanketed by ash flows erupted during regionally extensive volcanic activity known as the ignimbrite flare-up (e.g., Epis and Chapin, 1974; Farmer et al., 2008). Lipman (2021) argued the Sawatch region's paleoelevation was high based on deep, rapid erosion of its flare-up volcanoes.

The late Eocene Mosquito Range and Arkansas Hills were cut by three major east-flowing

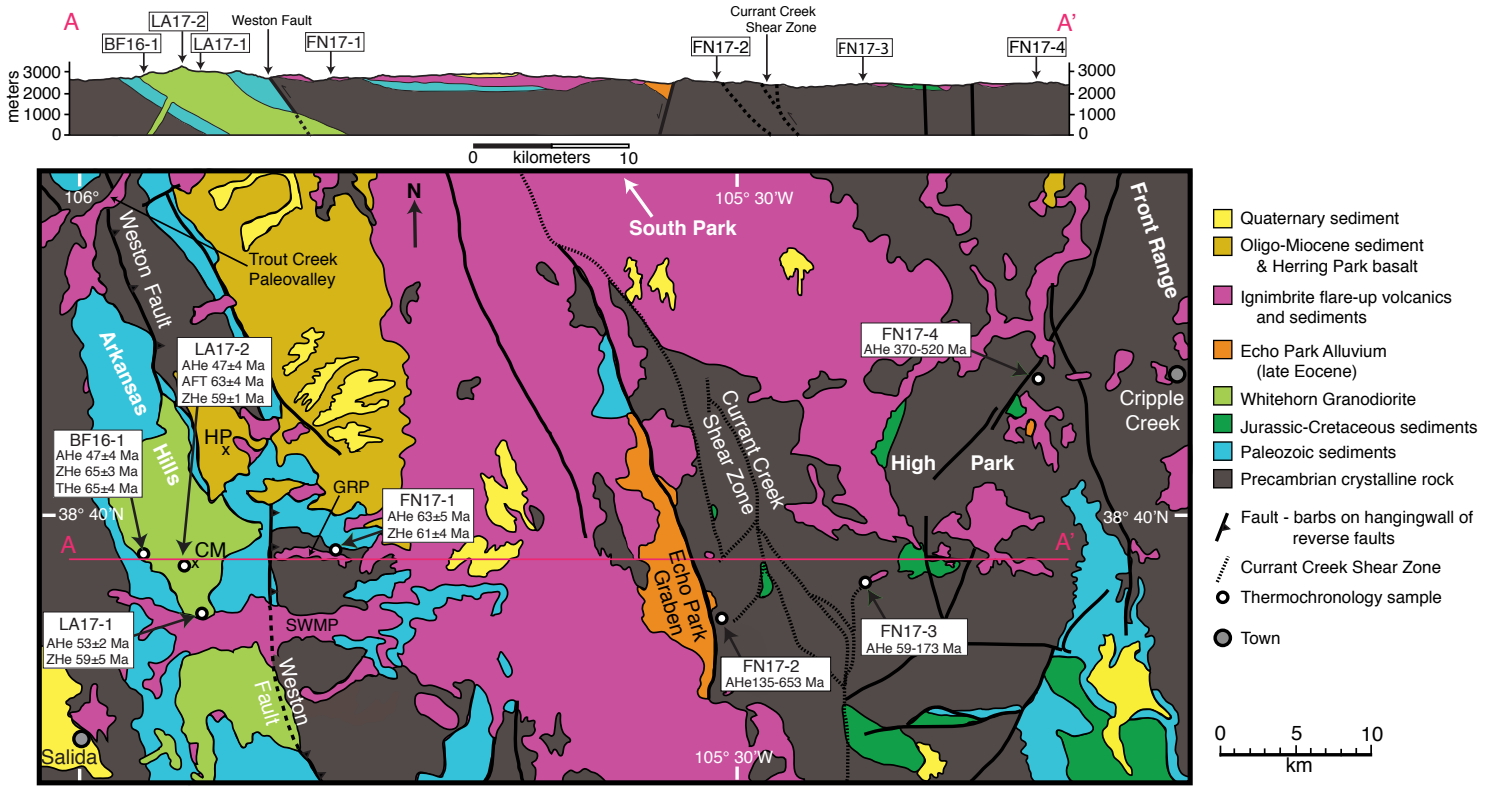

Figure 3. Geologic map and cross section of the Arkansas Hills–High Park study area. The red line on the map shows the location of cross-section A–A′. Thermochronology samples labeled with white dots. Sample names and thermochronologic dates for each system are shown for each sample. The South Park portion of the South Park–High Park intermontane basin lies northwest of the map area, as shown. CM—Cameron Mountain, with the "x" marking the summit; HP—"x" Herring Park, with the "x" marking the park; SWMP—Salida-Waugh Mountain paleovalley; GRP—Gribbles Run paleovalley.

paleovalleys that filled with sediments and ash-flow tuffs as old as 38 Ma (McIntosh and Chapin, 2004). The three paleovalleys are, from north to south, the Buffalo Peaks, Trout Creek, and Salida–Waugh Mountain (Figs. 1 and 3). The Salida-Waugh Mountain valley cuts the Whitehorn Granodiorite (Figs. 2, 3, and 4A); the valley possessed of >450 m of late Eocene topographic relief to the top of Cameron Mountain, composed of that granodiorite (Fig. 4A; Wallace et al., 1997; Wallace and Lawson, 2008).

An early, extensive flare-up ash flow is the 36.7 Ma Wall Mountain Tuff (WMT), whose source lies in the Sawatch Range near the Mount Princeton batholith (Fig. 1; McIntosh and Chapin, 2004). The WMT flowed east through all the paleovalleys, across the RMES, and spilled onto the Great Plains at Castle Rock (Figs. 1 and 2), 120 km to the east. The WMT is not significantly displaced across the Rockies–Great Plains interface, so post–37 Ma differential uplift between the provinces has been minimal (Leonard and Langford, 1994). Several studies have combined the province-spanning nature of the WMT with paleofloral characteristics in the 34.1 Ma Florissant Formation immediately above to deduce paleoelevations, and hence the timing of epeirogenic uplift, in central Colorado. Unfortunately, their paleoelevation estimates do not agree. Meyer (1992), Gregory and Chase (1992) and Wolfe et al. (1998) concluded the RMES at Florissant (Fig. 1) stood at its current 2.5 km elevation by 34 Ma, meaning epeirogenic uplift must be late Eocene or older. Other workers, using similar data but different techniques, concluded that Florissant stood then at 300–900 m; epeirogenic uplift elevated it to its current height more recently (MacGinitie, 1953; Trimble, 1980; Cather et al., 2012; Zaborac-Reed and Leopold, 2016). Clearly, other methods must be employed to deduce epeirogenic uplift timing.

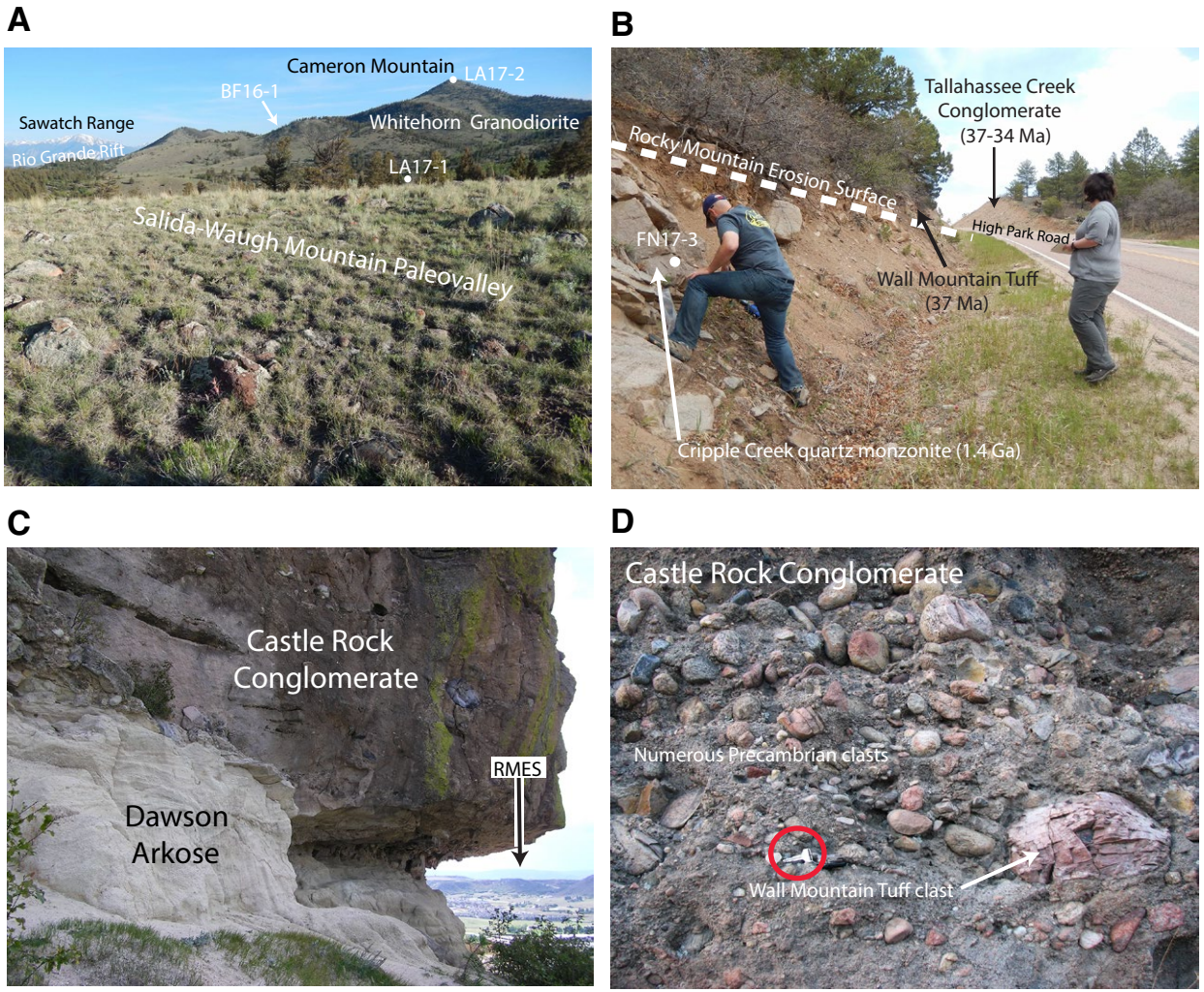

Figure 4. Study area photos. (A) View looking northwest from the Salida-Waugh Mountain paleovalley to Cameron Mountain. Locations of the three Whitehorn Granodiorite samples are marked. The BF16-1 location is hidden behind Cameron Mountain's south ridge. The Sawatch Range, the western portion of the Laramide-age Sawatch anticline, is visible on the horizon to the upper left, separated from the Arkansas Hills by the Upper Arkansas Valley, which is part of the Rio Grande Rift. (B) View of FN17-3 sample location, looking east. FN17-3 consists of 1.4 Ga quartz monzonite immediately below the Rocky Mountain Erosion Surface (RMES). Wall Mountain Tuff directly overlies the RMES in this location, with Tallahassee Creek Conglomerate overlying the tuff. (C) View looking southwest from Rock Park in the town of Castle Rock. The Castle Rock boulder conglomerate unconformably overlies the Dawson Arkose. The distant mountain skyline is the Rampart Range, the summit of which comprises the Rocky Mountain Erosion Surface (RMES). (D) Close-up photo of the Castle Rock Conglomerate in Castlewood Canyon State Park (deposited between 37 and 34 Ma). The Wall Mountain Tuff (37 Ma) had already experienced erosion, as revealed by the tuff clast shown. Almost all other clasts consist of sub-rounded to rounded Precambrian gneiss and granite. Car key for scale circled in red.

Development of the Rio Grande Rift (RGR)

Colorado's stress field evolved from compression to extension during the Oligocene. Normal faults began to dismember the RMES by 28 Ma (e.g., Scott, 1975; Landman and Flowers, 2013). Several Laramide ranges were bisected by RGR half-grabens (Kellogg, 1999). The Sawatch anticline was split by growth of the Upper Arkansas Valley half-graben, separating the Arkansas Hills from the rest of the anticline (Figs. 1 and 4A). Two thermochronologic studies in the Sawatch Range tracked exhumation associated with rifting (Ricketts et al., 2016; Abbey and Niemi, 2018), but the large magnitude of the RGR signal there obscures the pre-RGR history, which is our focus. The Arkansas Hills, in the half-graben's hangingwall, did not experience RGR-associated exhumation, making them an ideal place to deduce that earlier history.

LOW-TEMPERATURE THERMOCHRONOLOGY

Description of the Technique and Discussion of Previous Work in the Arkansas Hills

The apatite, zircon and titanite (U-Th)/He (AHe, ZHe, and THe) techniques and apatite fission-track (AFT) method are thermochronologic tools to resolve thermal histories for rocks below ~200 °C. These thermal histories can be used to infer exhumation histories through the upper ~5–7 km of the crust based on assumptions about the upper-crustal thermal field.

The (U-Th)/He method is based on the decay of U, Th, and Sm to He, and on volume diffusion of He out of the crystal lattice. At low temperatures, the crystal retains all He; at high temperatures, it is completely lost; and at intermediate temperatures, He is partially retained in what is known as the He partial retention zone (PRZ; Fig. 5). The temperature range of He retention depends on the mineral, its amount of radiation damage (Shuster et al., 2006), and on crystal size (Reiners and Farley, 2001). Apatite is sensitive to ~30–60 °C for low-damage crystals, increasing to ~110 °C for high-damage apatite (Farley, 2000; Flowers et al., 2009). For zircon and titanite, low-damage crystals begin to retain He at ~210 °C (Fig. 5; e.g., Reiners and Farley, 1999; Reiners et al., 2002; Stockli and Farley, 2004). Damage accumulation first increases temperature sensitivity in zircon; then, at higher levels, decreases it (in both zircon and titanite) to <50 °C (Guenthner et al., 2013; Baughman et al., 2017).

Effective uranium concentration (eU) is used as a proxy for radiation damage for grains of the same mineral that underwent the same thermal history (eU weighs the decay of U and Th by their He production, and is computed as eU = U + 0.235 * Th). Depending on the time-temperature (tT) path and the eU range of the mineral suite, positive (apatite and zircon), negative (zircon and titanite), or flat (apatite, zircon, and titanite) date-eU relationships occur (e.g., Shuster et al., 2006; Flowers et al., 2007; Guenthner et al., 2013). He diffusion kinetic models that track the evolution of mineral He retentivity with radiation damage accumulation and annealing are available for apatite (e.g., Flowers et al., 2009; Gautheron et al., 2009) and zircon (e.g., Guenthner et al., 2013), and can be used to quantitatively model the thermal history significance of (U-Th)/He results (e.g., Ketcham, 2005; Gallagher, 2012).

The basis of the apatite fission-track method is the accumulation of fission tracks in the crystal lattice from spontaneous nuclear fission of ^{238}U, and on temperature-dependent annealing of those tracks. At temperatures above the partial annealing zone (PAZ; Fig. 5), ~120 °C, fission tracks anneal immediately. Within the PAZ, down to ~60 °C, tracks are progressively shortened (partially annealed; from initially ~16 µm length). At temperatures below the PAZ, accumulated tracks are preserved (e.g., Fleischer et al., 1975; Gleadow and Fitzgerald, 1987; Donelick et al., 1990). Track annealing rates depend primarily on the temperature but also on factors such as heating and/or cooling rate, chemistry (in apatites), track orientation, and radiation

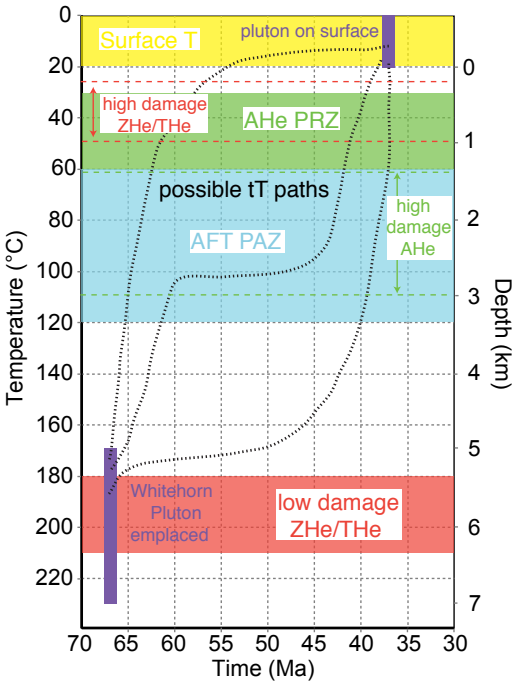

Figure 5. Schematic diagram to illustrate the approximate temperature and burial depth ranges through time probed by each of the thermochronometers used in this study. Temperature is converted to depth here assuming a surface temperature of 20 °C and a geothermal gradient of 30 °C/km. The ~210–180 °C range of ZHe and THe temperature sensitivity for grains with low amounts of radiation damage is shown in orange; the ~50–30 °C ZHe and THe sensitivity for high-damage grains lies between the orange dashed lines. The ~120–60 °C apatite fission-track (AFT) partial annealing zone (PAZ) is shown in blue, and the ~60–30 °C AHe partial retention zone (PRZ) for low-damage grains is in green. The higher-temperature AHe sensitivity for high-damage apatite grains lies between the green dashed lines. The range of surface temperatures (T) is shown in yellow. The emplacement depth of the Whitehorn pluton at 67 Ma is shown in purple, as is the arrival of the pluton at the surface by 37 Ma. The black dashed lines schematically represent example theoretical pluton time-temperature (tT) paths that we tested via HeFTy tT modeling (Fig. 8) using the thermochronometers depicted here.

damage. A kinetic parameter, the mean of a grain's maximum diameter of fission-track etch pits (D_{par}), can indicate how readily the tracks anneal (e.g., Carlson et al., 1999). Determining spontaneous fission-track density and the mineral U content allows calculation of the time since track accumulation started. The distribution of confined track lengths indicates the integrated thermal history of the mineral (e.g., review by Donelick et al., 2005, and references therein).

A previous exhumation study in the Arkansas Hills included zircon U/Pb, hornblende and biotite $^{40}Ar/^{39}Ar$, and AHe analyses of the Whitehorn Granodiorite and AHe and ZHe analyses of nearby Precambrian samples (Abbey et al., 2017). The overlap at ca. 67 Ma in zircon U/Pb and all $^{40}Ar/^{39}Ar$ dates was used to infer Whitehorn pluton emplacement and rapid cooling to T <300 °C at that time. These results and existing stratigraphic estimates (Wofford,1986) imply that the Whitehorn pluton was emplaced at 5–7 km depth at 67 Ma, then subsequently exhumed (Abbey et al., 2017). In contrast, pre–67 Ma AHe dates for lower Arkansas River samples (east of Coaldale; Fig. 1) indicated less exhumation to the east. Whitehorn Granodiorite AHe dates in the Abbey et al. (2017) study were not fully reproducible. This led the authors to disregard these data when interpreting the exhumation history of the Arkansas Hills and to instead attribute sample age dispersion to partial resetting from passage of ignimbrites through the paleovalleys.

Sampling Strategy

Three of our four Arkansas Hills samples are Whitehorn Granodiorite. The samples span the 447 m elevation range of Whitehorn exposure, from the Salida–Waugh Mountain paleovalley (2899 m) to the top of Cameron Mountain (3346 m; Figs. 2, 3, and 4A). The fourth sample (2688 m) is Precambrian granodiorite from the Gribbles Run paleovalley (Figs. 2 and 3). All three High Park samples are Precambrian granitoids collected at elevations between 2433 and 2508 m (Figs. 2 and 3).

The Whitehorn Granodiorite presents two advantages for our study. First, its Cretaceous age means its apatite crystals have accumulated less radiation damage than Proterozoic rocks, thus they have lower He retentivity. Consequently, Whitehorn AHe should detect lower exhumation magnitudes than will basement samples. Second, the Whitehorn's thermal and exhumation history is shorter and simpler than that of Proterozoic basement, making its interpretation less complex. See Stanley et al. (2013, 2015) for an example of this approach in southern Africa.

All our samples either directly underlie the 37 Ma Wall Mountain Tuff or are from Cameron Mountain, which is cut by the tuff-filled Salida–Waugh Mountain paleovalley (Figs. 3 and 4A). Therefore, every sample was on Earth's surface by 37 Ma. This knowledge greatly restricts the time interval during which any thermochronologically detected exhumation event could have transpired.

Methods

Mineral separation was done at the University of Colorado using standard crushing, water table, magnetic, and heavy-liquid techniques. Single crystals of zircon, titanite, and apatite were then hand-picked for (U-Th)/He analysis based on crystal size, shape, and absence of inclusions using a microscope with polarized transmitted and reflected light. All (U-Th)/He analyses were done in the University of Colorado Thermochronology Research and Instrumentation Lab (CU TRaIL). Detailed analytical methods are described in the Supplemental Material[1].

Sample mean (U-Th)/He data are reported in Table 2, (U-Th)/He single-grain data in Table 3, and additional data details in Table S1 (footnote 1). Analytical uncertainties on single-grain dates are reported at 2σ and include propagated analytical uncertainties on the parent and daughter isotope measurements. We assign a conservative 15% uncertainty on single-crystal eU values based on past work (e.g., Guenthner et al., 2013; Baughman et al., 2017). Where sample means are noted in the text and in Table 2, the associated uncertainty is reported as the 1σ sample standard deviation.

Fission-track dating of apatites was done at the University of Tübingen using the external detector and zeta-calibration techniques (Hurford, 1990). Apatites were mounted in epoxy resin, ground, polished, etched (for 20 s in 5.5 M HNO_3 at 21°C), and covered with mica external detectors for irradiation. Samples were irradiated, together with Durango and Fish Canyon Tuff age standards and IRMM540 uranium dosimeter glasses, at the FRM-II nuclear reactor (Garching, Germany). After irradiation, micas were etched in 40% HF for 30 min at room temperature. Fission tracks were counted, and confined tracks and D_{par} were measured at 1000× power using a Zeiss AxioImager microscope with AutoScan software. Five D_{par} measurements were conducted for each grain, where track density was known and/or confined track lengths were measured. Table 4 is a summary of AFT data, including AFT pooled ages, mean confined track lengths, and D_{par}. Single-grain data used in thermal history modeling are in Tables S2 and S3 (footnote 1).

Results for Cretaceous Whitehorn Granodiorite Samples from the Arkansas Hills

To accomplish our goal of reconstructing the Whitehorn pluton's cooling and erosion history between its 67 Ma time of emplacement and its surface exposure by 37 Ma, we acquired ten ZHe dates and 20 AHe dates from all three Whitehorn samples, six THe dates from one sample, and AFT dates and track-lengths for two samples (Tables 2–4, S1–S3, footnote 1).

The individual ZHe dates range from 69 to 55 Ma, overlapping with or slightly younger than pluton emplacement age. Dates show no correlation with eU (55–337 ppm; Fig. 6A). Samples yield mean ZHe dates of 65 ± 3 Ma, 59 ± 1 Ma, and 59 ± 5 Ma for BF16-1, LA17-2, and LA17-1, respectively. Six single-grain THe dates from BF16-1 are 72–61 Ma

[1]Supplemental Material. Contains additional information about samples and their thermochronologic analysis, analytical methods used, HeFTy modeling, and comparison of results with those from previous work on Whitehorn granodiorite. Please visit https://doi.org/10.1130/GEOS.S.19294217 to access the supplemental material, and contact editing@geosociety.org with any questions.

TABLE 2. SAMPLE LOCATION AND HELIUM DATA

Sample name	Longitude (°W)	Latitude (°N)	Elevation (m)	Apatite mean date (Ma)	1σ standard deviation in apatite date (Ma)	Zircon mean date (Ma)	1σ standard deviation in zircon date (Ma)	Titanite mean date (Ma)	1σ standard deviation in titanite date (Ma)
Arkansas Hills									
LA17-2	105.9156	38.6297	3346	46.9	3.7	59.2	1.1	—	—
BF16-1	105.9425	38.6352	2939	47.4	4.2	65.0	3.3	64.8	4.1
LA17-1	105.9028	38.6072	2899	52.6	1.8	58.7	4.9	—	—
FN17-1	105.7879	38.6407	2688	62.9	5.4	60.9[a]	3.8	—	—
Sample name	Longitude (°W)	Latitude (°N)	Elevation (m)	Apatite date range (Ma)[b]					
High Park									
FN17-2	105.5165	38.6024	2433	135–653					
FN17-3	105.4086	38.6267	2508	59–173					
FN17-4	105.2811	38.7536	2488	370–520					

[a]Grain z04 date is omitted from the mean and standard deviation (see text).
[b]Youngest and oldest grain dates listed here. See Table 3 for all grain dates.
Note: Dash denotes no data for that system.

(eU = 49–102 ppm). The mean THe date of 65 ± 4 Ma overlaps with the sample's ZHe date.

We acquired AFT data for two samples, but only one (LA17-2) yields a reliable result. The AFT date for LA17-2 (24 measured grains) is 63 ± 4 Ma (1σ; Fig. 6A; Tables 4 and S2, footnote 1) and overlaps with pluton emplacement. The mean track length is 13.6 ± 2.1 µm (1σ; Table 4) with a unimodal distribution (Table S3). The latter indicates that no reheating occurred once the sample cooled below PAZ temperatures. While the rather long mean track length suggests that the sample did not remain within the PAZ for an extended length of time, the relatively wide track length distribution also indicates that cooling did not occur rapidly. Note however that only 27 confined track lengths could be measured (not the typical goal of 100) and that the sample's thermal history is not well constrained from these results. Single-grain D_{par} range between 2.9 and 5.3 µm, and single-grain dates do not correlate with D_{par} (Table S2). The relatively high mean D_{par} of 3.8 ± 0.6 µm (Table 4) suggests comparatively high resistance to track annealing and, thus, a high closure temperature (e.g., Carlson et al., 1999; Donelick et al., 2005). The AFT date for BF16-1 is 79 ± 4 Ma from 20 measured grains (Tables 4 and S2, footnote 1) and is significantly older than the 67 Ma U/Pb emplacement age. Many grains showed curved dislocations in the crystal lattice when etched. Based on the pluton crystallization age, we consider the AFT data for sample BF16-1 unreliable and do not use them in the subsequent analysis.

The 20 single-grain AHe dates from the three samples are all distinctly younger than pluton emplacement and vary from 55 to 41 Ma. The dates are uncorrelated with eU (13–43 ppm eU range; Fig. 6B), crystal size (Fig. S1A, footnote 1), or sample elevation (Fig. 6C). Sample mean dates and uncertainties overlap and are 53 ± 2 Ma, 47 ± 4 Ma, and 47 ± 4 Ma for LA17-1, LA17-2, and BF16-1, respectively. Our AHe data are reproducible both within and between all samples. This contrasts with some AHe data reported previously for the Whitehorn Granodiorite (Abbey et al., 2017), as discussed in the Comparison with Previous Work on the Whitehorn Granodiorite section of the text file in Supplemental Materials. Based on the reproducibility of our AHe results, we consider them reliable; they faithfully record the cooling and exhumation history of the constituent rocks.

Results for Precambrian Granodiorite Sample from the Arkansas Hills

We acquired ZHe and AHe data for a 1.67 Ga Arkansas Hills granodiorite, FN17-1, collected 10 km east and 211 m lower than LA17-1 to compare with data from the nearby Whitehorn pluton. Three ZHe grain dates are reproducible (64–57 Ma) and uncorrelated with eU (793–961 ppm, Fig. 7A). The mean 61 ± 4 Ma date overlaps the Whitehorn ZHe dates. A high eU grain (1747 ppm) has a 39 Ma ZHe date, likely due to radiation-damage enhanced loss of He retentivity (Fig. 5; Guenthner et al., 2013). Four AHe dates are 70–59 Ma for a 46–166 ppm eU range (Fig. 7A). The 63 ± 5 Ma mean AHe date overlaps sample FN17-1's ZHe date and is older than AHe dates for the nearby Whitehorn samples.

Results for Precambrian Basement Samples from the High Park area

The 18 AHe dates for three Precambrian High Park samples (Figs. 3 and 6B; Tables 2 and 3) allow assessment of spatial heterogeneity of the

TABLE 3. SINGLE-GRAIN (U-Th)/He DATA

Sample name and aliquot[a]	Rs (μm)[b]	^{4}He (nmol/g)[c]	±[d]	U (ppm)[c]	±[d]	Th (ppm)[c]	±[d]	Sm (ppm)[c]	±[d]	eU[e]	±[f]	Uncorrected date (Ma)[g]	Uncorrected date Analytic (uncorrected) (Ma) 2σ[h]	F_T comb[i]	Corrected date (Ma)[j]	Corrected date Analytic (uncorrected) (Ma) 2σ[h] (Ma) 2σ[k]
Apatite																
BF16-1																
BF16-1_a01	84.9	3.46	0.00	10.4	0.1	34.8	0.7	85.1	1.4	18.8	2.8	34.1	0.4	0.82	41.4	0.8
BF16-1_a02	79.4	3.14	0.01	8.0	0.1	30.7	0.6	101.6	2.9	15.4	2.3	37.8	0.4	0.81	46.5	1.1
BF16-1_a03	80.9	3.50	0.01	11.3	0.2	33.0	0.6	89.2	3.5	19.2	2.9	33.8	0.4	0.81	41.4	1.0
BF16-1_a04	64.2	3.59	0.01	9.7	0.2	37.6	0.5	146.2	4.6	18.8	2.8	35.2	0.5	0.77	45.9	1.3
BF16-1_a05	55.0	4.10	0.01	11.1	0.2	38.9	0.8	150.9	4.0	20.5	3.1	37.0	0.5	0.73	50.7	1.3
BF16-1_a06	76.3	3.09	0.01	9.3	0.2	28.9	0.3	93.1	4.2	16.3	2.4	35.0	0.4	0.80	43.5	1.1
BF16-1_a07	50.7	4.57	0.01	10.6	0.4	51.1	0.9	141.7	8.3	22.9	3.4	36.9	0.7	0.70	52.4	1.9
BF16-1_a08	49.3	6.20	0.02	14.4	0.6	72.6	1.1	143.5	6.8	31.8	4.8	36.1	0.7	0.69	51.8	1.9
BF16-1_a09	46.3	3.22	0.01	8.6	0.4	35.2	0.7	153.6	7.7	17.2	2.6	34.7	0.8	0.68	50.9	2.3
BF16-1_a10	42.9	7.57	0.02	15.2	0.5	116.3	1.6	251.8	13.9	43.2	6.5	32.5	0.5	0.65	50.1	1.5
FN17-1																
FN17-1_a01	52.9	24.16	0.10	65.3	1.1	159.3	1.8	520.1	15.8	103.8	15.6	43.1	0.5	0.72	59.7	1.4
FN17-1_a02	46.3	43.13	0.09	107.8	1.1	244.8	3.4	537.0	7.5	166.6	25.0	47.9	0.4	0.68	69.9	1.1
FN17-1_a03	59.5	11.98	0.06	29.1	0.6	68.5	0.6	273.3	4.5	45.7	6.8	48.6	0.6	0.75	64.5	1.7
FN17-1_a04	62.7	14.20	0.06	42.6	0.4	64.8	0.5	298.7	6.5	58.4	8.8	45.0	0.4	0.77	58.6	1.0
FN17-2																
FN17-2_a01	56.9	38.59	0.10	22.3	0.4	16.4	0.2	486.4	8.3	26.8	4.0	261.6	3.9	0.75	345.8	10.8
FN17-2_a02	65.3	18.23	0.03	14.6	0.2	7.0	0.1	398.5	7.9	16.7	2.5	199.0	2.7	0.78	252.2	6.8
FN17-2_a03	60.1	50.26	0.08	17.8	0.3	10.2	0.2	417.4	4.7	20.7	3.1	433.1	6.6	0.76	559.4	17.0
FN17-2_a04	73.4	6.00	0.02	8.7	0.1	3.1	0.0	302.9	4.5	9.8	1.5	112.9	1.1	0.81	138.9	2.6
FN17-2_a05	58.9	12.12	0.04	12.8	0.2	6.5	0.1	422.4	5.3	14.8	2.2	150.0	2.4	0.76	195.7	6.2
FN17-2_a06	69.2	30.18	0.08	22.3	0.3	11.6	0.2	420.3	3.9	25.5	3.8	215.3	2.2	0.79	269.3	5.6
FN17-2_a07	65.5	78.26	0.17	22.8	0.3	13.8	0.3	553.0	5.7	26.8	4.0	518.9	5.8	0.78	653.4	14.9
FN17-3																
FN17-3_a01	66.0	14.37	0.04	27.1	0.3	5.0	0.2	175.9	3.5	28.5	4.3	92.8	1.0	0.79	117.8	2.6
FN17-3_a02	63.8	5.50	0.02	11.1	0.2	2.4	0.2	210.3	3.5	12.0	1.8	84.8	1.4	0.78	108.3	3.7
FN17-3_a03	43.6	9.07	0.04	17.0	0.4	4.5	0.5	298.7	7.2	18.4	2.8	90.8	2.2	0.68	132.6	6.1
FN17-3_a04	60.2	14.63	0.04	18.7	0.4	4.7	0.2	244.1	4.3	20.1	3.0	133.5	2.3	0.76	173.4	6.0
FN17-3_a05	49.9	2.09	0.02	8.4	0.2	2.0	0.3	158.7	7.2	9.1	1.4	42.4	1.1	0.72	58.7	2.9
FN17-3_a06	64.5	10.02	0.04	35.3	0.6	3.8	0.2	251.0	4.8	36.6	5.5	50.7	0.9	0.78	64.7	2.2
FN17-4																
FN17-4_a01	58.9	36.70	0.08	20.0	0.6	4.8	0.2	315.1	7.2	21.5	3.2	307.5	8.8	0.76	400.0	22.8
FN17-4_a02	47.0	58.51	0.17	26.3	0.8	6.6	0.3	350.9	3.5	28.3	4.2	370.9	10.5	0.70	520.0	29.6
FN17-4_a03	55.0	26.85	0.05	15.1	0.3	4.6	0.1	305.2	2.8	16.5	2.5	293.6	4.8	0.74	390.0	12.7
FN17-4_a04	62.0	42.94	0.09	24.4	0.6	8.2	0.1	454.2	8.5	26.9	4.0	288.6	6.1	0.77	370.3	15.3
FN17-4_a05	40.3	45.99	0.11	24.0	1.2	6.3	0.1	499.8	12.9	26.1	3.9	317.6	14.6	0.65	475.8	43.8
LA17-1																
LA17-1_a01	72.5	6.97	0.04	20.2	0.6	40.3	1.3	258.1	2.5	30.1	4.5	42.8	0.9	0.80	53.7	2.3
LA17-1_a02	49.4	3.73	0.05	13.0	0.2	25.2	0.3	265.1	4.3	19.3	2.9	35.8	0.6	0.70	50.5	1.6
LA17-1_a03	63.8	4.01	0.02	13.0	0.2	22.6	0.5	188.8	1.8	18.6	2.8	39.9	0.6	0.77	51.6	1.4
LA17-1_a04	67.4	3.06	0.02	8.4	0.2	18.6	0.2	190.2	2.2	13.1	2.0	43.2	0.7	0.78	55.2	1.7
LA17-1_a05	48.7	4.51	0.03	15.7	0.2	28.1	0.4	309.7	5.9	22.7	3.4	36.7	0.5	0.70	52.1	1.3

(*continued*)

TABLE 3. SINGLE-GRAIN (U-Th)/He DATA (*continued*)

Sample name and aliquot[a]	Rs (μm)[b]	^{4}He (nmol/g)[c]	±[d]	U (ppm)[c]	±[d]	Th (ppm)[c]	±[d]	Sm (ppm)[c]	±[d]	eU[e]	±[f]	Uncorrected date (Ma)[g]	Uncorrected date Analytic (uncorrected) (Ma) 2σ[h]	F_T comb[i]	Corrected date (Ma)[j]	Corrected date Analytic (uncorrected) (Ma) 2σ[h] (Ma) 2σ[k]
LA17-2																
LA17-2_a1	40.0	3.31	0.05	13.4	0.3	39.0	0.7	291.6	11.9	23.0	3.5	26.6	0.6	0.63	41.8	1.7
LA17-2_a2	37.1	5.93	0.04	24.7	0.6	62.9	0.8	323.2	5.6	40.1	6.0	27.4	0.5	0.61	44.9	1.5
LA17-2_a3	38.7	5.48	0.04	20.9	0.4	55.0	0.8	280.0	12.2	34.3	5.1	29.6	0.4	0.62	47.3	1.4
LA17-2_a4	48.6	8.51	0.04	25.3	0.5	77.4	0.6	327.8	6.8	44.0	6.6	35.8	0.4	0.70	51.3	1.2
LA17-2_a5	46.3	4.69	0.04	15.6	0.3	41.1	0.6	339.4	11.5	25.8	3.9	33.7	0.5	0.68	49.1	1.5
Zircon																
BF16-1																
BF16-1_z05	65.7	55.33	0.06	165.1	1.5	60.1	0.9	7.0	16.9	179.4	26.9	57.0	0.5	0.82	69.4	1.2
BF16-1_z06	41.6	19.39	0.03	55.8	1.2	80.0	1.6	0.0	0.0	74.9	11.2	47.9	0.8	0.71	67.3	2.2
BF16-1_z07	52.3	18.69	0.04	55.9	0.7	74.5	1.8	12.8	36.9	73.6	11.0	47.0	0.5	0.77	61.0	1.3
BF16-1_z08	52.1	14.73	0.03	41.8	1.0	56.6	1.2	0.0	0.0	55.2	8.3	49.4	0.9	0.77	64.2	2.2
BF16-1_z09	56.1	73.47	0.08	247.7	3.8	87.0	2.6	0.0	0.0	268.4	40.3	50.6	0.7	0.79	64.0	1.8
FN17-1																
FN17-1_z01	78.1	270.79	0.61	915.8	8.0	193.4	1.4	40.3	1.9	961.7	144.3	52.0	0.4	0.85	61.2	1.0
FN17-1_z02	82.5	315.05	1.04	1637.3	13.7	464.9	3.9	86.0	0.7	1747.8	262.2	33.4	0.3	0.86	38.9	0.6
FN17-1_z03	49.3	247.08	0.48	878.1	11.4	210.2	36.9	28.1	4.3	928.1	139.2	49.2	0.8	0.76	64.5	2.0
FN17-1_z05	53.0	190.03	0.36	724.5	15.5	289.9	26.6	56.2	2.9	793.4	119.0	44.3	0.9	0.78	56.9	2.3
LA17-1																
LA17-1_z01	76.0	66.50	0.40	152.3	2.2	480.0	3.2	n.m.	n.m.	266.5	40.0	46.2	0.5	0.84	55.2	1.2
LA17-1_z02	63.9	91.90	0.60	261.4	6.0	317.6	3.1	n.m.	n.m.	337.0	50.6	50.4	0.9	0.80	62.1	2.3
LA17-2																
LA17-2_z01	77.0	34.29	0.09	100.0	0.9	110.6	20.7	4.8	0.9	126.2	18.9	50.2	2.0	0.84	59.5	4.8
LA17-2_z02	75.7	29.80	0.10	90.4	0.8	95.6	1.9	5.0	0.3	113.1	17.0	48.7	0.4	0.84	57.9	1.0
LA17-2_z03	70.4	41.19	0.10	123.6	1.4	123.4	1.0	5.8	0.6	152.9	22.9	49.8	0.5	0.83	60.0	1.1
Titanite																
BF16-1																
BF16-1_ttn01	27.1	35.14	0.06	35.8	0.6	347.2	5.6	28.8	0.6	118.3	17.7	55.0	0.7	0.84	65.3	1.5
BF16-1_ttn02	23.3	47.12	0.05	38.5	0.5	445.4	8.9	34.7	0.9	144.4	21.7	60.4	0.9	0.83	72.4	2.0
BF16-1_ttn03	31.7	35.32	0.05	29.6	0.4	311.9	4.6	34.1	0.8	103.7	15.6	63.0	0.7	0.87	72.4	1.6
BF16-1_ttn04	20.8	52.54	0.05	56.5	1.2	543.2	8.9	80.7	2.3	185.6	27.8	52.4	0.7	0.79	66.1	1.6
BF16-1_ttn05	21.5	45.41	0.04	45.7	0.8	476.5	6.4	55.6	2.6	159.0	23.8	52.9	0.6	0.81	65.4	1.3
BF16-1_ttn06	19.6	49.24	0.07	48.4	0.6	519.1	9.8	86.4	4.6	171.7	25.8	53.1	0.7	0.79	66.8	1.7

Note: n.m.—not measured.
[a]Sample and mineral being analyzed. a is apatite; z is zircon.
[b]Rs is the radius of a sphere with an equivalent alpha ejection correction as the grain, calculated using equation A6 in Cooperdock et al. (2019).
[c]Concentrations of He, U, Th, and Sm computed from their absolute amounts and the estimated dimensional mass reported in Table 3.
[d]2σ propagated analytical uncertainty on the U, Th, Sm, and He measurements.
[e]eU is effective uranium concentration. Calculated as U + 0.2375*Th + 0.0012*Sm.
[f]Uncertainty on eU estimated at 15% of the eU value.
[g]Date is calculated iteratively using the ^{4}He production equation defined as equation 1 in Wolfe et al. (1998) and assuming secular equilibrium.
[h]2σ propagated analytical uncertainty on the U, Th, Sm, and He measurements.
[i]The combined alpha-ejection correction for the crystal calculated from the isotope specific fission-track corrections in Table 2, the proportion of U and Th contributing to ^{4}He production, and assuming homogeneous parent isotope distributions.
[j]The corrected date is calculated iteratively using the absolute values of He, U, Th, and Sm in Table 2, the isotope specific fission-track corrections in Table 2, and equation 34 in Ketcham at al. (2011) assuming secular equilibrium.
[k]2σ propagated analytical uncertainty on the U, Th, Sm, and He measurements.

TABLE 4 SUMMARY OF APATITE FISSION-TRACK (AFT) DATA FOR WHITEHORN GRANODIORITE SAMPLES

Sample name	No. of grains dated	Ns[a]	Ni[a]	ρs (tracks/cm^2)[b]	ρi (tracks/cm^2)[b]	P(χ)2 (%)[c]	ρd (tracks/cm^2)[d]	1σ ρd error (%)	Nd[e]	AFT pooled date (Ma)[f]	1σ date error (Ma)[f]	Number of lengths measured	Mean length, SD (μm)[g]	Mean D_{par}, ±1σ (μm)[h]
BF16-1	20	939	1437	7.15E+05	1.08E+06	61	9.45E+05	1.51	4375	78.7	3.6	150	12.91 ± 2.49	2.29 ± 0.12
LA17-2	24	350	658	3.45E+05	6.30E+05	25	9.36E+05	1.55	4140	63.2	4.4	27	13.60 ± 2.09	3.76 ± 0.55

Note: The AFT age of sample BF16-1 is older than the pluton's crystallization age and considered unreliable and not used in the interpretation and thermal modeling (see text for details). Single-grain details can be found in Tables S2 and S3 (text footnote 1).

[a]Ns/Ni: number of spontaeneous/induced tracks counted.

[b]ρs/ρi: spontaneous/induced track density.

[c]P(χ)2: chi-square probability (if >5%, the sample passes the test, and grain ages are considered to be from the same population).

[d]ρd: induced track density in the external detector over the dosimeter glass (with 15 ppm uranium concentration).

[e]Nd: number of tracks counted to determine ρd.

[f]Pooled age and 1σ error determined using the zeta calibration technique (zeta and standard error of 256.8 ± 5.0 a*cm^2 for BF16-1 and 255.4 ± 4.2 a*cm^2 for LA17-2).

[g]Mean of confined track lengths with related standard deviation (SD).

[h]Mean sample D_{par} (maximum diameter of fission-track etch figure parallel to the c-axis) with related standard deviation.

regional thermal history. The AHe dates are almost all pre-Laramide, and intrasample variability is high. Samples have positive date-eU correlations (Fig. 7B), consistent with the expected increase in He retentivity with greater radiation damage (Flowers et al., 2009) but have no correlation with crystal size (Fig. S1B, footnote 1). Dates are 653–135 Ma (N = 7) for FN17-2, 173–59 Ma (N = 6) for FN17-3, and 520–370 Ma (N = 5) for FN17-4.

DISCUSSION

Thermal History—Evidence for Eocene Exhumation Caused by Epeirogeny

Our primary goal is to constrain the post-Laramide cooling and erosion history of the study area. Because the High Park samples were incompletely reset in the Mesozoic, they cannot resolve that history. For that reason, we briefly discuss the High Park data and then focus on the implications of the Arkansas Hills samples for post-Laramide exhumation.

High Park Thermal History—Spatial Heterogeneity in Burial Magnitudes

The pre–Western Interior Seaway (WIS) AHe dates for High Park samples limit maximum temperatures to <110 °C since Laramide time, meaning burial depths of <~2.5–3 km. By contrast, Arkansas Hills ZHe and THe dates are Laramide or younger, so temperatures were >180 °C (burial >5 km) when the Laramide orogeny began. This east-to-west depth increase reinforces Abbey et al.'s (2017) conclusion that Cenozoic exhumation is greater west of Coaldale (Fig. 1).

The cumulative WIS and Laramide sedimentary thickness in South Park, 70 km north of High Park exceeds 4.5 km (Barkmann et al., 2016). Thus, the maximum 2.5–3 km post-WIS basement burial depth for our High Park samples requires significant southward thinning of WIS and/or Laramide synorogenic sedimentary strata, consistent with Cross and Pilger's (1978) WIS isopach map.

Arkansas Hills: Thermal History Reveals Eocene Exhumation

Thermal history from data patterns. In contrast to the High Park samples, our Arkansas Hills data enable detailed interpretation of the Laramide and younger thermal and exhumation history. Comparison of the multiple thermochronometer results for the Whitehorn samples implies a multiphase cooling and erosion history in the 30 m.y. between 67 Ma pluton emplacement and surface exposure by 37 Ma. The general overlap of ZHe, THe, and AFT dates with crystallization age indicates an initial episode of rapid Paleocene cooling from magmatic temperatures down to temperatures less than ~120 °C based on the AFT results. Eocene AHe dates for all samples suggest a second cooling phase, from ~120 °C to the surface, during the Eocene.

The Arkansas Hills Precambrian basement sample (FN17-1), collected 10 km east of the Whitehorn samples (Fig. 3), likely has a similar thermal history, but its AHe date (63 ± 5 Ma) is older. This disparity in AHe dates is likely because the sample's Precambrian apatite grains have higher He retentivity (i.e., higher closure temperature) than the Whitehorn apatite due to a longer interval of radiation damage accumulation (Fig. 5; Flowers et al., 2009).

Thermal history modeling. We conducted thermal history modeling to quantitatively evaluate evidence for an Eocene cooling signal in the Arkansas Hills samples (Fig. 8). Our inverse time-temperature (tT) thermal history models use the HeFTy software (Ketcham, 2005), RDAAM annealing model (Flowers et al., 2009) for apatite He diffusion kinetics, ZRDAAM annealing model (Guenthner et al., 2013) for zircon He diffusion kinetics, and the model of Ketcham et al. (2007) for apatite fission-track annealing kinetics. We do not include THe data because there is no titanite radiation damage model, but the overlap of our THe and ZHe dates means their inclusion would not impact model results. HeFTy supports a maximum of seven date inputs; we grouped the AHe and ZHe dates into bins of similar eU and used the average

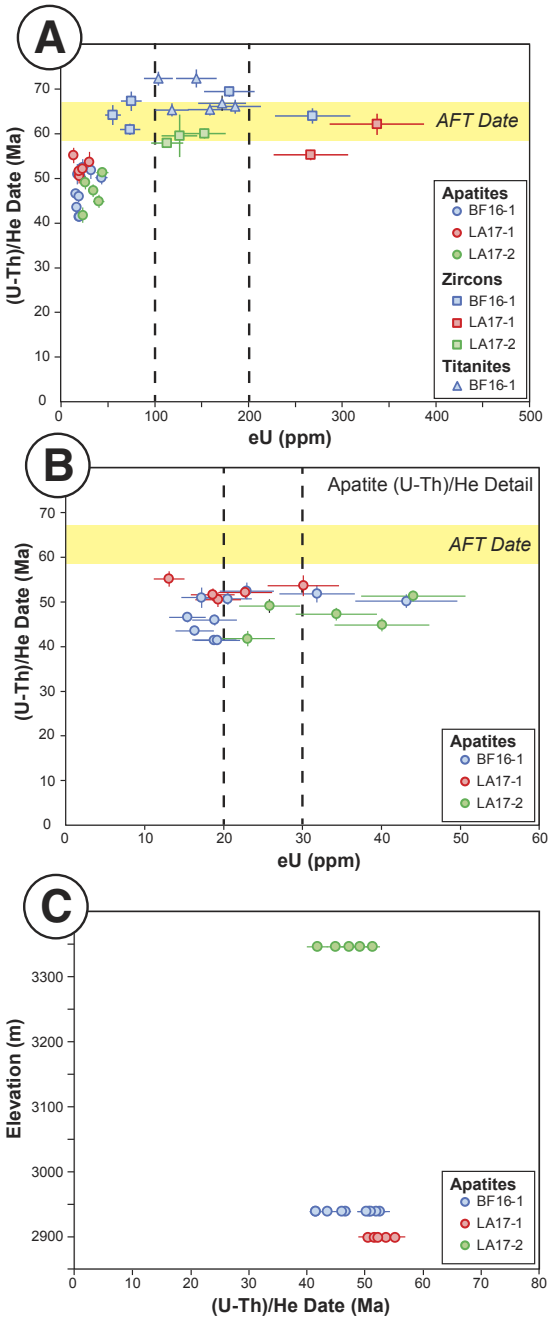

Figure 6. Thermochronometric data for samples of Whitehorn Granodiorite. (A) Plot of ZHe, THe, AFT, and AHe dates versus effective uranium (eU) contents for all grains in the Whitehorn Granodiorite samples. Yellow band shows the 2σ AFT date range for LA17-2. (B) Detail of the 0<eU<60 ppm portion of the plot in (A) to better show the AHe data, which has a lower eU than zircon and titanite. Vertical dashed lines on both (A) and (B) separate the eU bins used for HeFTy modeling. (C) Plot of date versus elevation for the three Whitehorn Granodiorite samples, showing that the dates are consistent across the entire 450 m elevation range.

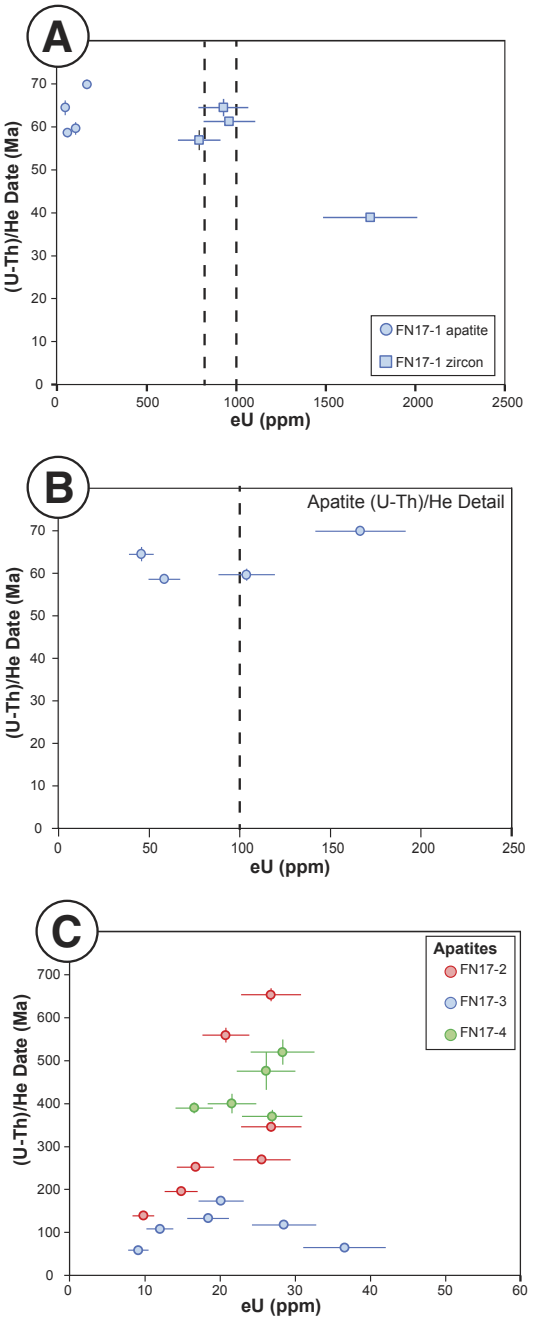

Figure 7. Thermochronometric data for Precambrian samples. (A) Plot of ZHe and AHe dates versus effective uranium (eU) contents for all grains in sample FN17-1, the Precambrian sample from the Arkansas Hills. The high eU zircon grain was not used in the HeFTy model of FN17-1 (Fig. 8D), as discussed in the text. (B) Detail of the 0<eU<250 ppm portion of the plot in (A) to better show the AHe data, which has a lower eU than zircon. Vertical dashed lines on both (A) and (B) separate the eU bins used for HeFTy modeling. (C) Plot of AHe dates versus effective uranium (eU) contents for all grains in the Precambrian samples from High Park.

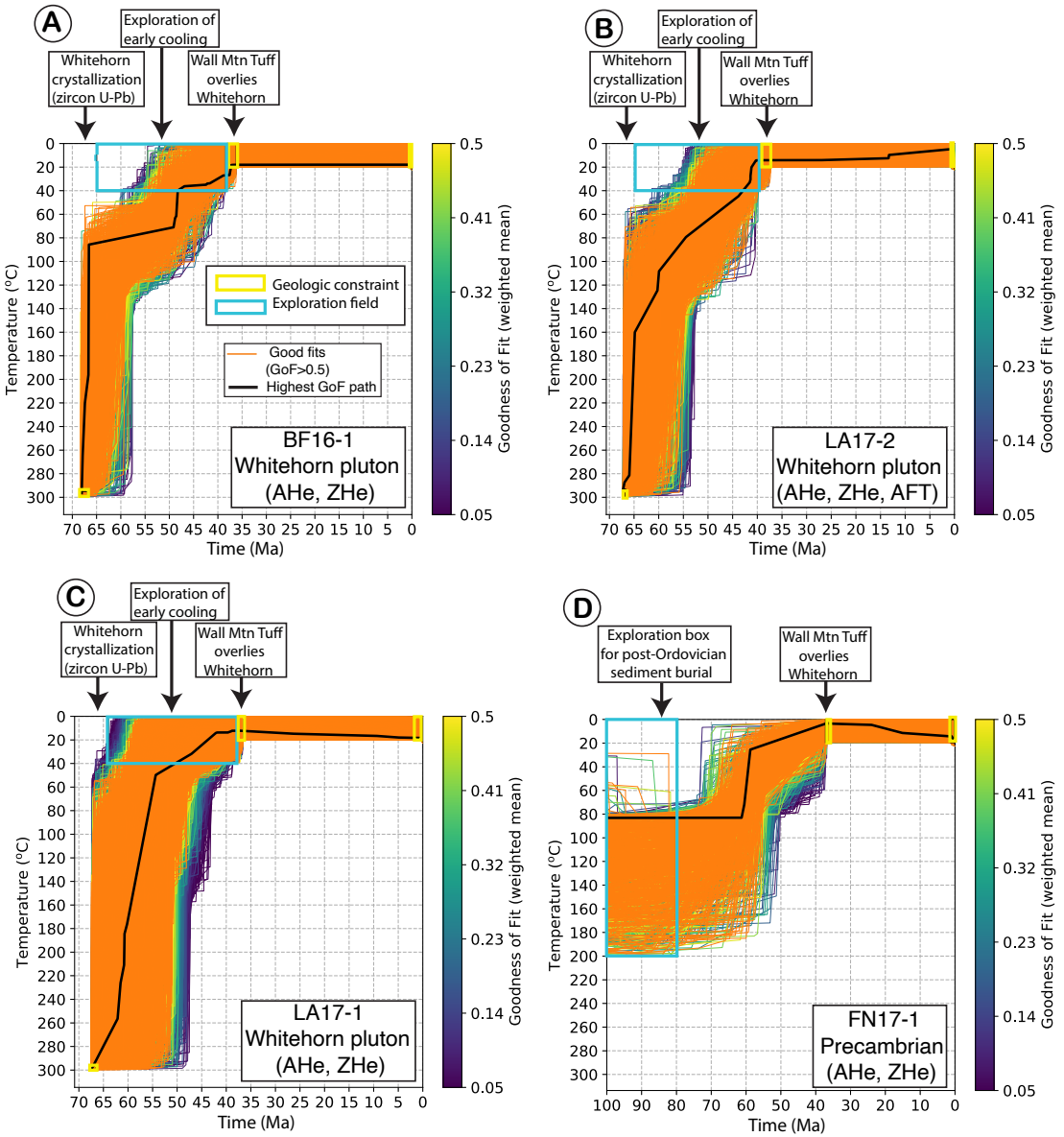

Figure 8. Time-temperature (tT) thermal models for the Arkansas Hills samples generated using HeFTy (Ketcham, 2005). The legend shown in panel A applies to all panels. The geologic constraints shown by yellow boxes, and the exploration fields shown by blue boxes are explained in the boxes at the top of the model. Orange paths are good fits (goodness of fit [GoF] >0.5); acceptable fits are shown using the color scale to the right of each plot, with the color corresponding to the GoF. The black line shows the statistically best fit of the 10,000 paths tried. See Figures 5 and 6 for the eU bins used as input for the HeFTy models and Table S4 (text footnote 1) for a summary of the modeling constraints used. See Figures 2 and 3 for the locations of all modeled samples. (A) Model for sample BF16-1. Rapid, Laramide-related cooling occurs from 67–60 Ma followed by slower cooling until sometime between 54–46 Ma, when a second episode of rapid cooling brings the sample to the surface by 37 Ma. (B) Model for sample LA17-2; (C) Model for sample LA17-1; (D) The last 100 m.y. (the relevant portion) of the full 1680 m.y. model duration for Precambrian sample FN17-1. See Figure S3 (text footnote 1) for the full 1680 m.y. model.

date, grain size, and eU of each bin as a separate input (Figs. 5A and 6A), which is a common HeFTy modeling strategy. AFT date and track length form another input. HeFTy tests the predicted dates for thousands of tT paths against the input data. Those paths that surpass a minimum goodness-of-fit threshold are deemed "good"—or "acceptable"—fits. Full model details are in Table S4 (footnote 1).

Figure 8 shows thermal history model results for ZHe, AFT, and AHe data for all four Arkansas Hills samples. Geologic constraints that we apply to all Whitehorn models (Figs. 8A–8C) are: (1) temperature (T) = 300 °C at 67 Ma (pluton emplacement); (2) cooling to surface T = 0–20 °C by 37 Ma (Wall Mountain Tuff contact); and (3) surface temperatures today. We add a T = 0–40 °C exploration box from 65 to 39 Ma to force HeFTy to test for Paleocene cooling to near-surface temperatures (Figs. 8A and 8B reveal that such early cooling is impossible for BF16-1 and LA17-2).

Figure 8D shows the last 100 m.y. of the Precambrian basement sample model (FN17-1). See Figure S3 (footnote 1) for the full 1680 Ma model. Geologic constraints we apply to this model (see Wallace et al., 1999) are: (1) T = 300 °C at t = 1672 Ma (pluton emplacement age); (2) cooling to T = 0–20 °C by t = 490–445 Ma (the age of the unconformably overlying Manitou Limestone); (3) return to surface T = 0–20 °C by t = 37 Ma (age of the overlying Wall Mountain Tuff); (4) surface T = 0–20 °C today. FN17-1 was buried by 5–8 km of Phanerozoic sediments after exposure on the surface in the Ordovician, so we apply an exploration box of T = 0–200 °C from t = 445–80 Ma to allow for reheating.

All tT paths with a goodness of fit (GoF) above 0.5 (labeled "good" paths in HeFTy) are shown in orange on Figure 8; the "best-fit" path is black. Paths with 0.05<GoF<0.5 (HeFTy's "acceptable" fits) are shown in progressively warmer colors for increasing GoF.

Thermochronologic Data Provide Evidence for a Separate Eocene Exhumation Episode

Do the quantitative tT models validate the above qualitative interpretation that the Arkansas Hills experienced two episodes of rapid cooling separated by an interval of slower cooling? Whitehorn samples BF16-1 and LA17-2 (Figs. 8A and 8B) place the tightest constraints on the cooling history—BF16-1 because its apatite and zircon grains span a wide eU range and LA17-2 because of its additional AFT constraint. In both cases, because HeFTy must honor data at multiple closure temperatures, the range of permissible paths is limited. Scrutiny of both tT models confirms the pluton's two-phase cooling history. The less constrained LA17-1 and FN17-1 (Figs. 8C and 8D) models are consistent; they permit but do not require two-stage cooling during the same interval.

For samples LA17-2 and BF16-1, the good-fit (orange) tT paths (Fig. 8) do not cool to <40 °C until after 54 Ma, thus yielding the two-phase cooling history and requiring substantial cooling between 54 Ma and surface conditions at 37 Ma. This significant phase of post–54 Ma cooling dictates the sinuous shapes of the orange fields in Figures 8A and 8B. Figure 9 shows that the best-fit paths for both samples predict grain dates that agree with measured dates, demonstrating the reliability of both models.

The orange field for BF16-1 contains 354 separate good paths, and LA17-2 has 618 of them (out of 10,000 paths attempted; Figs. 8A and 8B), making it impossible to trace individual paths across the entire tT history. Each good path represents an equally plausible tT history, so our two-stage cooling interpretation requires demonstration that *all* good paths exhibit two-stage cooling, not just some of them. To facilitate the tracing of complete paths, we plotted 40 randomly selected good paths for BF16-1 in gray on Figure 10A. Every path defines a two-stage cooling history, with one rapid cooling episode in the Paleocene and one in the Eocene. Figure 10B shows the same result for 40 different randomly selected BF16-1 paths. Figures 10C and 10D show different randomly selected paths for LA17-2—all display two-stage cooling. The evidence for two-stage cooling is robust.

Tracking the field of good fits shows that the pluton cooled to between 120 and 60 °C by 60 Ma when cooling slowed. Part of this cooling must be due to postemplacement thermal relaxation, but 120–60 °C is unreasonably cool for the 5–7 km emplacement depth, so Laramide exhumation must also play a role. Assuming today's 30 °C/km geothermal gradient (Berkman and Watterson, 2010) and surface T = 10–20 °C, the pluton lay ~1.3–3.7 km below the surface at 60 Ma. Thus, the Arkansas Hills experienced ~1.3–5.7 km of exhumation between 67

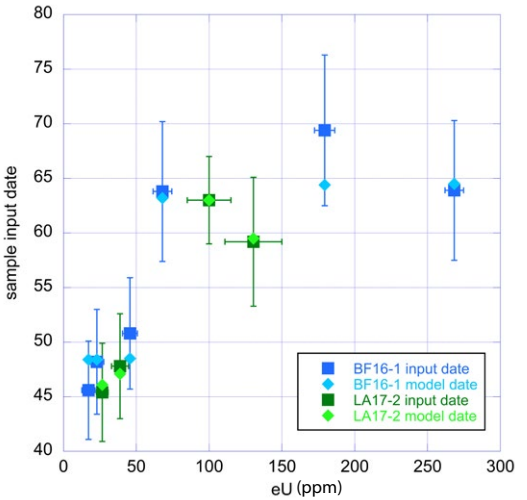

Figure 9. Plot that compares each model input date (i.e., the average date for all grains in a bin) for each apatite or zircon eU bin with the simulated date for that bin calculated for the best-fit model for the samples that place the strongest constraints on the time-temperature (tT) history, BF16-1 (blue) and LA17-2 (green). The apatite fission-track (AFT) date for LA17-2 is independent of eU, but we plot it (arbitrarily) at eU = 100 to represent it with the rest of the data. Measured dates are shown with square symbols and error bars; best-fit model dates by diamonds. Notice that the modeled date lies within the uncertainty for every input data point, demonstrating that the modeled good-fit paths reproduce the data well.

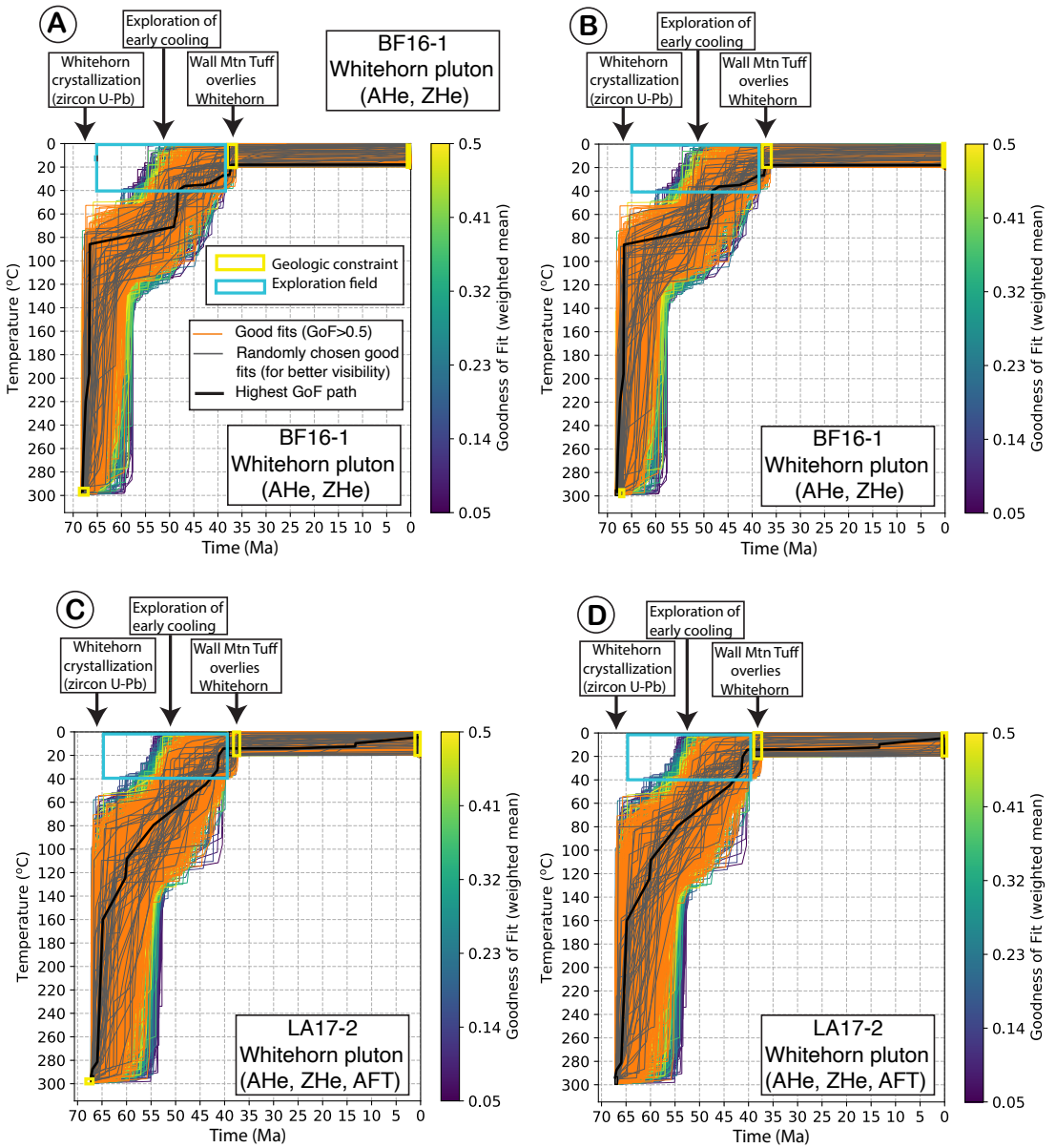

Figure 10. The same time-temperature (tT) models for samples BF16-1 and LA17-2 as shown in Figure 8 but with 40 randomly selected good paths plotted in gray. All other good paths are orange, as in Figure 8. This color difference allows the full tT trajectory of individual good paths to be followed more easily than is possible in Figure 8. Notice that each randomly selected path displays a two-stage cooling history, as discussed in the text. The legend shown in panel A applies to all panels. (A) BF16-1 with 40 randomly selected good paths shown in gray. (B) BF16-1 with a different 40 randomly selected paths shown in gray. (C) LA17-2 with 40 randomly selected good paths shown in gray. (D) LA17-2 with a different 40 randomly selected paths shown in gray.

and 60 Ma. This thermal modeling result showing that rapid Laramide erosion ended by 60 Ma is consistent with sedimentary evidence that the Sawatch anticline stopped supplying sediment to South Park at that time (Barkmann et al., 2016).

After an episode of comparatively slow cooling between ca. 60–54 Ma, a second phase of rapid cooling began sometime between 54 and 46 Ma; the pluton was exhumed from ~1.3–3.7 km depth at the start of this episode and reached the surface by 37 Ma. Laramide crustal shortening was not responsible for this Eocene exhumation because the locus of shortening had moved east of the Sawatch anticline by that time. We attribute it, instead, to epeirogeny.

Eocene Changes in Basin Sedimentation Patterns—Evidence for Epeirogeny

The onset of epeirogenic rock uplift could trigger the kilometer-scale, Eocene Arkansas Hills exhumation documented by the tT models, but thermochronology alone cannot constrain the duration of the epeirogeny, and our data pertain to one small area—epeirogeny, by definition, affects a broad region. The sedimentary histories of the South Park–High Park and Denver basins (Fig. 1) provide four strong arguments for the simultaneous onset of Eocene erosion in those basins *and* the Arkansas Hills, a hallmark of epeirogeny, and that the epeirogeny affected central Colorado sedimentation patterns into the Oligocene. These four arguments are: (1) development of basin-wide unconformities simultaneous with onset of Arkansas Hills exhumation; (2) subsequent deposition of late Eocene conglomerate; (3) cut-and-fill architecture in subsequent deposits; and (4) missing synorogenic strata in the Laramide basins. Here we examine each argument.

Eocene Unconformities in Laramide Basins

Accommodation space was created by subsidence of the South Park–High Park Basin throughout deposition of the 69–56 Ma South Park Formation, the basin's synorogenic fill (Barkmann et al., 2016). In South Park, an unconformity separates the South Park Formation from 38.2 Ma tuff (McIntosh and Chapin, 2004); therefore, the unconformity spans 56–38 Ma. Any South Park Formation deposited in High Park was eroded during this unconformity (Figs. 2 and 4B).

The Denver Basin exhibits an unconformity that spans the same time interval. The basin's Laramide synorogenic fill (Figs. 2 and 4C) has a confusing history of name changes; most recently, Thorson (2011) called it the Denver Basin Group. It is ~900 m thick and was deposited between ca. 69–54 Ma (Hicks et al., 2002). An unconformity internal to the Group exists on the basin edges, but the missing middle-late Paleocene strata exist in the basin's center (Thorson, 2011), revealing that subsidence produced accommodation space continuously during the orogeny until 54 Ma, the age of the upper Dawson Arkose, the Group's stratigraphically highest formation.

Near Castle Rock, the Denver Basin Group fills the basin almost to the level of the RMES on the adjacent Front Range (Figs. 1 and 2). The oldest unit overlying the Dawson Arkose is the Larkspur Conglomerate (Thorson, 2011). Detrital zircon ages reveal the Larkspur to be younger than 41 Ma (Koch et al., 2018), and it underlies the 37 Ma Wall Mountain Tuff. Thus, the Denver Basin unconformity spans the time range of 54 Ma to 41–37 Ma.

In summary, unconformities in South Park (56–38 Ma) and the Denver Basin (54–41 Ma) are contemporaneous with Arkansas Hills exhumation (Table 1), demonstrating that post-Laramide exhumation affected both Laramide highlands and basins, a hallmark of epeirogeny.

Deposition of Post-Laramide Conglomerates

When deposition resumed at 41–37 Ma in the Denver Basin, the sedimentary system's energy level was considerably higher than it was at the end of Laramide deposition. The maximum grain size in the Dawson Arkose is 1.5 cm; the overlying Larkspur Conglomerate contains rounded granitic clasts to 20 cm (Thorson, 2011). The Larkspur contains few volcanic clasts (Koch et al., 2018), and it underlies the Wall Mountain Tuff, the first extensive ignimbrite flare-up deposit. Because this rise in transport energy manifests in the pre-volcanic Larkspur Conglomerate, the rise of ignimbrite flare-up volcanic topography could not be its cause.

Although the names of clastic units differ in South Park–High Park, their characteristics mirror those of the Denver Basin, documenting that late Eocene high-energy conditions predated the flare-up. The oldest sedimentary unit overlying the South Park Formation is the Echo Park Alluvium, of likely late Eocene age (Epis and Chapin, 1974). It fills paleochannels and two small grabens (Figs. 2 and 3; Epis and Chapin, 1974; Wobus and Epis, 1978; Epis et al., 1979). It is an analog for the Larkspur Conglomerate in that it largely lacks volcanic clasts and underlies the Wall Mountain Tuff.

Many workers concluded that Colorado's late Eocene topography possessed low relief (e.g., Epis and Chapin, 1975), but ubiquitous low relief is incompatible with widespread deposition of late Eocene conglomerate (Evanoff, 1990). As noted above, Arkansas Hills paleovalleys had >450 m of late Eocene relief. Trimble (1980) appealed to surface uplift at that time to explain conglomerate deposition. Eaton (2008) argued that today's SRM ranges are erosional remnants of their Laramide predecessors that sit atop the crest of an ~1500-m-tall epeirogenic dome (Fig. 11). Late Eocene rise of this dome, with the Sawatch anticline piggybacked atop, would increase local relief, thus raising transport energy, facilitating the cutting of paleovalleys, and depositing conglomerate long *after* the Laramide orogeny ended and *before* ignimbrite flare-up volcanism.

Cut-and-Fill Sedimentary Architecture—Evidence for an Absence of Accommodation Space

Laramide sediments in both the Denver and South Park–High Park basins consist of basin-spanning units that record contemporaneous basin subsidence; accommodation space was continually produced during the orogeny. When deposition

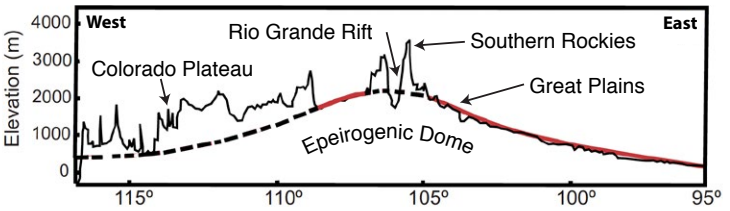

Figure 11. Topographic profile across the Colorado Plateau, Southern Rocky Mountains (SRM), and Great Plains at 36°N latitude in black and the trace of the epeirogenic dome inferred by Eaton (2008) shown in red. Surface uplift of the dome would rejuvenate erosion in the SRM, which piggyback atop the crest of the dome. The westward rise of the Great Plains delineates the eastern flank of the dome. Modified from Eaton (2008).

resumed after the early-middle Eocene unconformities, accommodation space was no longer being created.

The late Eocene units in High Park illustrate this cut-and-fill architecture. They fill abundant paleochannel remnants that reveal a south- and east-flowing drainage system like the one that drained the Laramide orogeny (Fig. 1; Epis and Chapin, 1975; Scott, 1975; Epis et al., 1976; Hills and Dickinson, 1982). This drainage pattern persisted through the late Eocene and early Oligocene, but individual channels frequently shifted, cutting previous deposits and filling with younger material. For example, the Echo Park Alluvium is the oldest unit overlying the RMES (Fig. 2), but the Wall Mountain Tuff directly rests on the RMES in many places (Fig. 4B). The Tallahassee Creek Conglomerate overlies the Wall Mountain stratigraphically, but post–Wall Mountain erosion resulted in the Tallahassee Creek directly overlying the Echo Park in places and the RMES elsewhere (Fig. 2; Epis and Chapin, 1974; McIntosh and Chapin, 2004).

The sedimentary record of the Denver Basin tells a similar story (Fig. 2). In places, the Larkspur Conglomerate, an Echo Park equivalent, rests unconformably on the Dawson Arkose, with the Wall Mountain Tuff above. Elsewhere, pre–37 Ma erosion removed the Larkspur; the Wall Mountain directly overlies the Dawson (Fig. 2). Post–37 Ma erosion removed both the Larkspur *and* Wall Mountain units elsewhere, leaving the Castle Rock Conglomerate unconformably above the Dawson (Figs. 2, 4C, and 4D; Thorson, 2011; Keller and Morgan, 2016).

Laramide Strata Is Missing in the Denver and High Park Basins

Gregory and Chase (1994) noted that Laramide crustal shortening should produce a Denver Basin deeper than 900 m—the thickness of the Denver Basin Group. They explained this seeming deficiency by ca. 54 Ma "emplacement of a buoyant subsurface load" under the basin (i.e., epeirogenic uplift). The Denver Basin Group is missing entirely from the northern basin; Cretaceous WIS units are overlain by the late Eocene White River Group (Tweto, 1979). Tweto (1975) interpreted this unconformity to reveal a Paleocene or Eocene rise of the Denver Basin. High Park is also missing the expected Laramide-age sediments, suggesting a similar history.

Summary

The relationships described here all suggest that central Colorado's east-southeast–flowing Laramide drainage system did not change appreciably during the Eocene, but a major change in drainage energy and style *did* occur. Active subsidence ceased in Laramide basins by 56–54 Ma, and erosion created unconformities. When deposition resumed at 41–37 Ma, the energy level had increased—*before* the growth of ignimbrite flare-up volcanic topography. These deposits exhibit a cut-and-fill architecture caused by the lack of accommodation space. What caused these changes plus contemporaneous Arkansas Hills exhumation? We favor Eocene epeirogeny, but we must entertain other possible causes before we can confidently draw that conclusion.

Potential Causes of Eocene Exhumation and Sedimentary Changes in Central Colorado

Molnar and England (1990) noted three possible causes for exhumation and conglomerate deposition: (1) drainage reorganization, (2) climate change, and (3) contemporaneous tectonism. Here we examine each candidate cause for Eocene central Colorado exhumation and conglomerate disposition.

Stream capture can increase a river's discharge, thereby increasing its erosional efficiency, leading to exhumation and/or conglomerate deposition. But, as noted above, central Colorado's drainage network (Fig. 1) changed little between the Laramide and the Oligocene (Scott, 1975; Epis et al., 1976); drainage reorganization is an unlikely cause of the area's Eocene changes.

Climate change can trigger accelerated erosion in a previously uplifted landscape. Workers have cited cooling events at the Eocene–Oligocene boundary (33.9 Ma), in the middle Miocene (ca. 15 Ma), and in the late Pliocene (ca. 3–4 Ma) as triggers for exhumation and conglomerate deposition (e.g., Molnar, 2004; Pelletier, 2009). But no abrupt change in climate that would likely trigger increased erosion coincides with central Colorado's Eocene changes (Fig. 12).

Three styles of tectonism could increase erosion in central Colorado: (1) crustal shortening, (2) crustal extension, and (3) epeirogenic surface uplift. As detailed above, Eocene crustal shortening did occur in Colorado but not in the Sawatch anticline; it cannot explain Arkansas Hills exhumation at that time. Similarly, high relief caused by extension fails as an explanation because the Rio Grande Rift formed later, in the Oligocene (Landman and Flowers, 2013; Ricketts et al., 2016).

Consideration of all possible mechanisms for Eocene central Colorado exhumation and conglomerate deposition leaves only one viable explanatory option—epeirogenic surface uplift.

Evidence for Eocene Epeirogeny from Previous Thermochronologic Studies

Several previous low-temperature thermochronologic studies have been conducted in central Colorado: Why didn't they detect Eocene epeirogeny? Here we posit that one AFT study *did* detect epeirogeny in the Sawatch Range, and another is suggestive for the northern Front Range. Bryant and Naeser (1980) concluded that three Eocene AFT dates from the Sawatch Range (51 and 52 Ma on two Precambrian rocks east of Aspen and 46 Ma from the 66 Ma West Tennessee Stock; see Fig. 1) "may represent an uplift event of regional significance during the Eocene that hitherto has been unknown" (p. 163). Epeirogeny is the most likely cause of this Eocene cooling; the reason, once again, is that crustal shortening ended in the Sawatch during the Paleocene.

Kelley and Chapin (2004) documented many 54–44 Ma (Eocene) AFT dates in the northern Front Range, including 50 Ma and 48 Ma dates for two samples near the town of Lyons (Fig. 1). Cenozoic evolution of the Front Range is complex; Kelley and Chapin (2004) attributed Eocene cooling there to a combination of Laramide crustal shortening, heating by Colorado Mineral Belt plutons, and thermal insulation from thick, low-conductivity Cretaceous shales—not epeirogeny. But Hoblitt and Larson (1975) argued that Laramide deformation ended before 63 Ma near Lyons. Reheating by Colorado Mineral Belt plutons is possible, but the nearest exposed pluton is 12 km away (Cole and Braddock, 2009); therefore, reheating was likely modest. Eocene epeirogeny provides an equally, or more, plausible explanation for the Eocene AFT dates near Lyons.

Combination of these AFT dates, the interpretation that Florissant (see Fig. 1 for location) had reached its current elevation by 34 Ma (Meyer, 1992; Gregory and Chase, 1992), rapid, deep erosion of Sawatch range flare-up volcanoes (Lipman, 2021), the Denver Basin unconformity, and our Arkansas Hills data allow us to draw a perimeter around the part of central Colorado that has evidence of Eocene epeirogeny (the red dashed line on Fig. 1). It measures ~170 km west-east (from Aspen to Castle Rock) by ~120 km north-south (from Lyons and the West Tennessee stock to the Whitehorn pluton). The affected area is >2.0 × 10^4 km^2, from the Sawatch Range to the Great Plains (Fig. 1).

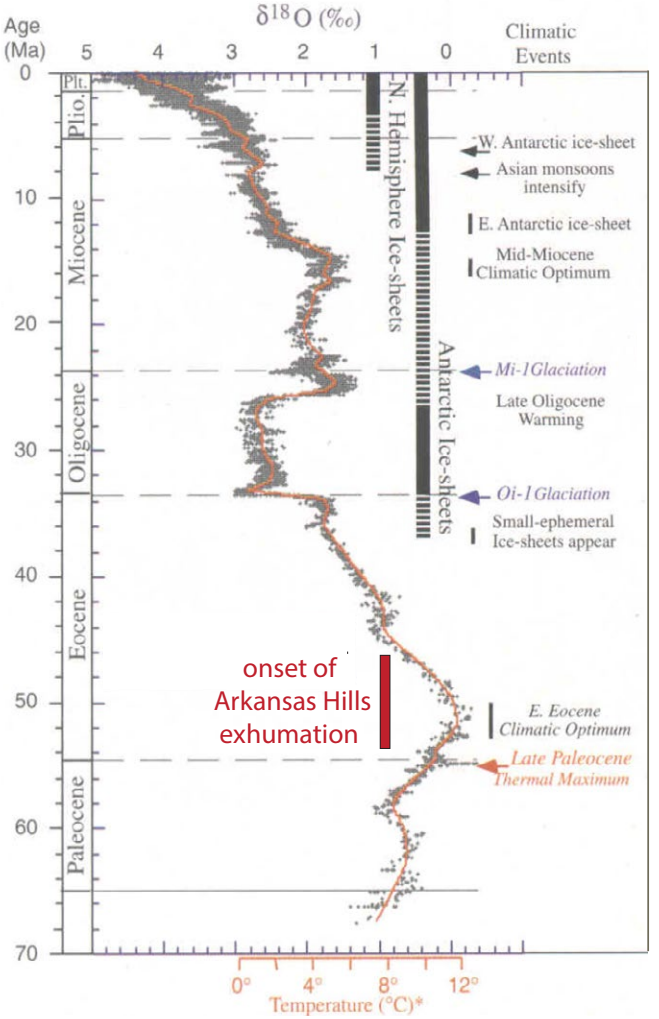

Figure 12. Reproduction of the Cenozoic deep-sea $\delta^{18}O$ record (Fig. 2 in Zachos et al., 2001). Data points are gray dots, and the orange line is the smoothed trend using a five-point running mean. Noteworthy climatic episodes highlighted by Zachos et al. (2001) are shown in black or orange, with full glacial episodes denoted by the black bars and ephemeral glacial episodes by the dashed black bars. We have shown the time of onset for Arkansas Hills exhumation in red. Notice that this exhumation coincided with the early Eocene Climatic Optimum followed by steady, gradual cooling. It does not coincide with any of the abrupt cooling episodes that have been suggested by others as causes for enhanced exhumation, as discussed in the text. Figure modified from Zachos et al. (2001).

What Epeirogenic Uplift Mechanism(s) Could Have Operated in the Eocene?

Here we explore the many options that could explain how central Colorado could rise

epeirogenically during the Eocene—both previously proposed mechanisms and a new hypothesis.

Viability of Previously Proposed Epeirogenic Uplift Mechanisms

Previously proposed mechanisms for epeirogenic uplift (and their implied timing) include: (1) removal of subcontinental lithosphere by a flat Farallon slab (syn- to immediately post-Laramide, ca. 70–35 Ma; Bird, 1988; Spencer, 1996); (2) de-densification of the subcontinental lithospheric mantle and/or continental crust by slab-derived fluids followed by slab removal (syn- to immediately post-Laramide, ca. 70–35 Ma; Humphreys et al., 2003; Jones et al., 2015); (3) delamination of underplated, eclogitized ignimbrite flare-up lower crust (post–35 Ma; Karlstrom et al., 2012; Lipman, 2021); (4) lithospheric thinning due to RGR extension (post–30 Ma; McMillan et al., 2002); (5) geologically recent mantle heating (ca. 10–5 Ma; Aslan et al., 2010; Karlstrom et al., 2012; Rosenberg et al., 2014); and (6) normal forces due to asthenospheric convection (i.e., dynamic topography); <10–5 Ma; Moucha et al., 2008; Becker et al., 2014; van Wijk et al., 2018).

Considering only the timing they imply, mechanisms 1 and 2 are viable explanations for Eocene epeirogeny in central Colorado. Mechanisms 3 through 6 all predict surface uplift *after* the Eocene. Therefore, none of them can explain the central Colorado epeirogeny, and we do not consider them further here; these mechanisms could have operated in other places at other times, though.

Bird (1988) proposed the shear traction hypothesis in part to explain a thicker SRM crust than could be produced by Laramide crustal shortening. Subsequent work (e.g., Sheehan et al., 1995) revealed that the SRM crust is no thicker than that beneath the adjacent Great Plains; the SRM are not supported by Airy isostasy as Bird (1988) envisioned. A further difficulty is that the model predicts complete removal of continental lithosphere, which several studies have shown remained beneath the region after the end of the Laramide orogeny (see Jones et al., 2011). So, although shear traction could explain the epeirogeny's timing, current understanding of the regional geology makes it an unlikely candidate.

Lee and Grand (1996) documented anomalously low seismic velocities beneath the SRM. They concluded that the mantle lithosphere is thin with hot, upwelled asthenosphere beneath the mountains. Seismology cannot detect the timing of upwelling. Others have suggested mantle heating is recent (Mechanism 5 above). Recent heating cannot explain our observations, but asthenospheric upwelling beginning ca. 54–46 Ma could (see the next section).

Humphreys et al. (2003) confirmed that low-velocity mantle underlies the SRM, but they attributed it to partial melt, not upwelled asthenosphere. They inferred that 200-km-thick lithosphere underlies the SRM; they explained high topography despite this thick lithosphere via hydration of the continental lithospheric mantle by fluids derived from the Farallon flat slab. Metasomatism de-densified the mantle lithosphere, causing epeirogenic uplift during the Laramide orogeny. A second epeirogenic episode followed at the end of the Laramide, caused by replacement of the sinking Farallon slab by asthenosphere—this timing fits our observations.

Jones et al. (2015) proposed a modified idea—that hydration de-densified the lower crust, not the mantle. This is an attractive explanation for the high elevation of the western Great Plains, which largely lack Cenozoic volcanism and are underlain by higher-velocity mantle.

The hydration hypothesis is appealing, but, assuming the Farallon slab dewaters uniformly, it predicts contemporaneous surface uplift everywhere above the flat slab. If such uplift triggered Eocene exhumation in central Colorado, one expects rocks elsewhere to record similar exhumation. That prediction is not supported by thermochronologic data from Colorado's Cenozoic plutonic rocks. As discussed below, kilometer-scale exhumation occurred in the Oligo-Miocene in the Spanish Peaks area and in the Miocene for the "Gothic Dome" (Fig. 1). No previous hypothesis, not even the hydration hypothesis, can explain well this diachronous exhumation across the SRM, leading us to suggest a new alternative—serial mantle drips.

A Newly Proposed Epeirogenic Uplift Mechanism—Serial Mantle Drips beneath Colorado

Houseman and Molnar (1997) considered the convective removal of mantle lithosphere via a Rayleigh-Taylor instability (i.e., a "mantle drip") to be an almost "inevitable" consequence of orogenic crustal thickening. Their numerical models revealed that non-Newtonian viscosity in olivine could cause delays of tens of millions of years between the end of shortening and the onset of a mantle drip. Mantle drips have been invoked to explain epeirogenic uplift episodes around the world, from the Sierra Nevada to the Andes to Tibet (e.g., Kay and Kay, 1993; Houseman and Molnar, 1997; Farmer et al., 2002; Jones et al., 2004; Ducea et al., 2013).

Our drip hypothesis posits that lithospheric thickening accompanied Laramide crustal thickening beneath the Sawatch and Front Ranges; lateral flow of viscous mantle lithosphere toward this small perturbation caused it to grow, first slowly, then exponentially (Figs. 13A and 13B). When the negatively buoyant drip detached in the Eocene, replacement with less dense asthenosphere produced epeirogenic surface uplift in central Colorado (Fig. 13C), resulting in Arkansas Hills exhumation, unconformities in the South Park–High Park and Denver basins, and conglomerate deposition. Because subsequent cooling of the asthenosphere to form thermal lithosphere occurs over tens of millions of years, the surface height produced by epeirogeny persists to the present.

Lower lithospheric heterogeneity created by the sinking of one drip can initiate formation of an adjacent drip, as Garzione et al. (2014) proposed to explain progressive surface uplift of the Bolivian Altiplano from south to north during the Miocene. Eocene removal of a mantle drip beneath central Colorado could plausibly trigger subsequent drips around its periphery. Lord et al. (2016) invoked an Oligocene drip to explain formation of multiple small-volume, ca. 25 Ma, alkaline magmatic centers in the Spanish Peaks area, ~170 km southeast of our study area (Fig. 1). Landman (2016) and Kainz et al. (2021) documented kilometer-scale exhumation of the Spanish Peaks and their surroundings a few

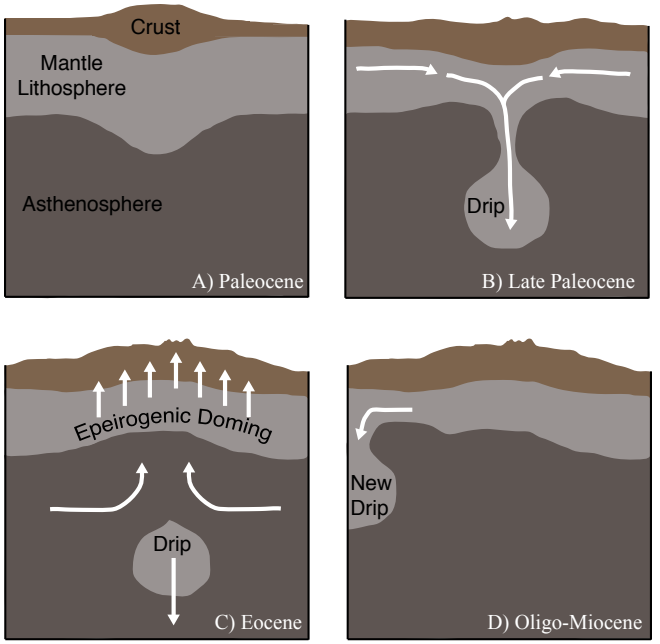

Figure 13. Cartoon illustration of the serial mantle drip hypothesis. (A) Paleocene: Laramide crustal shortening produces lithospheric thickening. (B) Late Paleocene: Viscous flow of continental mantle lithosphere toward the thickened portion creates a gravitationally unstable lithospheric mantle "drip." (C) Eocene: The drip detaches and sinks, thus thinning the originally thickened portion of the mantle lithosphere. Less dense asthenosphere replaces the drip. Isostatic adjustment to the new, lower density column produces regional surface uplift by epeirogenic doming. (D) Oligo-Miocene: Thicker lithosphere now surrounds the thinned mantle beneath the Eocene epeirogenic dome. Relief on the lithosphere-asthenosphere boundary triggers a new episode of lateral flow of lithosphere, seeding a subsequent lithospheric drip adjacent to the original Eocene one.

million years after pluton emplacement. Activity of an Oligo-Miocene drip could explain both observations (Fig. 13D).

The "Gothic Dome," in the Elk and West Elk ranges near Aspen, abuts the region of Eocene exhumation (Fig. 1). AHe, ZHe, and AFT data (Garcia, 2011; Abbott et al., 2021) record >4 km of Miocene exhumation in the center of the ~100-km-diameter dome, with the magnitude of exhumation tapering to near zero outside the dome's perimeter. Samples surrounding the dome all have much older AHe dates. We suggest that an Eocene drip east of Aspen could have spawned a Miocene drip southwest of Aspen—the latter produced the Gothic Dome (Fig. 13D).

Does the area's lithospheric structure support the mantle drip hypothesis? Xenoliths derived from the shallow mantle lithosphere (<75 km depth) exist in 8 Ma basalt from Herring Park, in our study area (Fig. 3; Bailley, 2010). This observation does not preclude the drip hypothesis, as Houseman and Molnar's (1997) numeric models show that drips typically remove only 50%–75% of the mantle lithosphere. The seismic velocity structure of the area is complex (e.g., Schmandt and Humphreys, 2010). Workers variously conclude that the lithosphere-asthenosphere transition lies at 200 km (Humphreys et al., 2003), 150 km (e.g., Hansen et al., 2013), or <100 km (e.g., Lee and Grand, 1996; Levander and Miller, 2012); seismic knowledge of lithospheric structure beneath Colorado is not sufficiently mature to rule the drip hypothesis in or out. We suggest, though, that the activity of serial drips might explain the area's seismic complexity and the presence of a "lithosphere-asthenosphere mixing zone" between ~80–200 km depth as hypothesized by Karlstrom et al. (2012).

CONCLUSIONS

Our analysis of the Arkansas Hills' Whitehorn pluton using ZHe, THe, AFT, and AHe thermochronometers allowed us to trace its thermal history between 67 Ma emplacement at 5–7 km depth and the surface by 37 Ma. The pluton experienced two episodes of rapid cooling. The first, between 67 and 60 Ma, was due to thermal relaxation combined with Laramide-induced exhumation. The pluton temperature was 60–120 °C (~1.3–3.7 km depth) at 60 Ma. Slow cooling ensued for the next 6–14 m.y. until a second episode of rapid cooling began between 54 and 46 Ma. Exhumation that brought the pluton to the surface by 37 Ma caused this Eocene cooling event.

Laramide crustal shortening ended in the Arkansas Hills by 67 Ma; therefore, it could not have caused the Eocene exhumation episode. Two central Colorado Laramide basins, the Denver and South Park–High Park, stopped subsiding and developed unconformities at 56–54 Ma, precisely when exhumation began in the Arkansas Hills. When deposition resumed at 41–37 Ma, transport energy was higher than during the late Laramide, and accommodation space was limited, suggesting regional uplift during unconformity development. We attribute simultaneous Arkansas Hills exhumation and formation of unconformities to the onset of Eocene epeirogenic doming of central Colorado. The dome was at least 170 km east-west by 120 km north-south, affecting >2.0 × 10^4 km^2 extending from the Sawatch Range to the western Great Plains.

Of the many hypotheses proposed to explain epeirogenic surface uplift in Colorado, hydration and de-densification of continental mantle lithosphere and/or crust by fluids released from the Farallon flat slab (Humphreys et al., 2003; Jones et al., 2015) is the best explanation for Eocene epeirogeny in central Colorado. But the hydration hypothesis has difficulty explaining a growing body of thermochronologic data that record kilometer-scale exhumation in different parts of Colorado at different times. This diachronous exhumation is better explained by convective removal of mantle lithosphere (i.e., mantle drips) at different times in different places. We suggest that an Eocene drip triggered epeirogeny in central Colorado. Relief on the lithosphere-asthenosphere boundary created by that drip seeded an Oligo-Miocene drip in the Spanish Peaks area and a Miocene drip in the Elk and West Elk Mountains.

ACKNOWLEDGMENTS

National Science Foundation (NSF) grant EAR-1559306 to Flowers and Metcalf provided support for new instrumentation during the course of this study that was used to acquire data in this project. Niazy thanks the NSF-funded RESESS program, run by UNAVCO, for the opportunity to work on this project. Abbott's ideas about central Colorado's evolution have benefitted from many discussions with Peter Molnar, Craig Jones, Lang Farmer, and Vince Matthews. We thank Peter Martin for help producing visualizations of HeFTy models that allow for visual tracking of individual time-temperature paths. We appreciate constructive reviews of an earlier version of this manuscript by Will Amidon and an anonymous reviewer and Associate Editor Greg Hoke's handling of the manuscript.

REFERENCES CITED

Abbey, A.L., and Niemi, N.A., 2018, Low-temperature thermochronometric constraints on fault initiation and growth in the northern Rio Grande rift, upper Arkansas River valley, Colorado, USA: Geology, v. 46, no. 7, p. 627–630, https://doi.org/10.1130/G40232.1.

Abbey, A.L., Niemi, N.A., Geissman, J.W., Winkelstern, I.Z., and Heizler, M., 2017, Early Cenozoic exhumation and paleotopography in the Arkansas River valley, southern Rocky Mountains, Colorado: Lithosphere, v. 10, no. 2, p. 239–266, https://doi.org/10.1130/L673.1.

Abbott, L.D., Flowers, R.M., Metcalf, J., Hiett, C., Kelleher, R., Camm, H., Ramba, M., McCorkel, N., and Riccio, E., 2021, The Gothic Dome: Kilometer-scale Miocene exhumation in Colorado's Elk and West Elk Mountains: Earth and Space Science Open Archive, https://doi.org/10.1002/essoar.10508533.1.

Aslan, A., Karlstrom, K.E., Crossey, L.J., Kelley, S., Cole, R., Lazear, G., and Darling, A., 2010, Late Cenozoic evolution of the Colorado Rockies: Evidence for Neogene uplift and drainage integration, *in* Morgan, L.A., and Quane, S.L., eds., Through the Generations: Geologic and Anthropogenic Field Excursions in the Rocky Mountains from Modern to Ancient: Geological Society of America Field Guide 18, p. 21–54, https://doi.org/10.1130/2010.0018(02).

Bailley, T.S., 2010, A reevaluation of the origin of Late Cretaceous and younger magmatism in the Southern Rocky Mountain region using space-time composition patterns in volcanic rocks and geochemical studies of mantle xenoliths [Ph.D. thesis]: Boulder, University of Colorado, 153 p.

Barkmann, P.E., Sterne, E.J., Dechesne, M., and Houck, K.J., 2016, South Park, Colorado: The interplay of tectonics and sedimentation creates one of Colorado's crown jewels, *in* Keller, S.M., and Morgan, M.L., eds., Unfolding the Geology of the West: Geological Society of America Field Guide 44, p. 151–190, https://doi.org/10.1130/2016.0044(07).

Baughman, J.S., Flowers, R.M., Metcalf, J.R., and Dhansay, T., 2017, Influence of radiation damage on titanite He diffusion kinetics: Geochimica et Cosmochimica Acta, v. 205, p. 50–64, https://doi.org/10.1016/j.gca.2017.01.049.

Becker, T.W., Faccenna, C., Humphreys, E.D., Lowry, A.R., and Miller, M.S., 2014, Static and dynamic support of western United States topography: Earth and Planetary Science Letters, v. 402, p. 234–246, https://doi.org/10.1016/j.epsl.2013.10.012.

Berkman, F.E., and Watterson, N.A., 2010, Interpretive Geothermal Gradient Map of Colorado: Colorado Geological Survey map MS-51, scale 1:500,000.

Bird, P., 1988, Formation of the Rocky Mountains, western United States: A continuum computer model: Science, v. 239, p. 1501–1507, https://doi.org/10.1126/science.239.4847.1501.

Bohannon, R.G., and Ruleman, C.A., 2013, Geologic map of the Mount Sherman 7.5′ quadrangle, Lake and Park counties, Colorado: U.S. Geological Survey Scientific Investigations Map 3271, scale 1:24,000.

Bryant, B., 1966, Possible window in the Elk Range thrust sheet near Aspen, Colorado, *in* Geological Survey Research 1966 Chapter D: U.S. Geological Survey Professional Paper 550-D, p. D1–D8.

Bryant, B., and Naeser, C.W., 1980, The significance of fission-track ages of apatite in relation to the tectonic history of the Front and Sawatch Ranges, Colorado: Geological Society of America Bulletin, v. 91, p. 156–164, https://doi.org/10.1130/0016-7606(1980)91<156:TSOFAO>2.0.CO;2.

Bryant, B., Marvin, R.F., Naeser, C.W., and Mehnert, H.H.,1981, Ages of igneous rocks of the South Park-Breckenridge region, Colorado, and their relation to the tectonic history of the Front Range uplift, Chapter C, in Shorter contributions to isotope research in the western United States, 1980: U.S. Geological Survey Professional Paper 1199, p. 15–26.

Carlson, W.D., Donelick, R.A., and Ketcham, R.A., 1999, Variability of apatite fission-track annealing kinetics: I. Experimental results: The American Mineralogist, v. 84, p. 1213–1223, https://doi.org/10.2138/am-1999-0901.

Cather, S.M., Chapin, C.E., and Kelley, S.A., 2012, Diachronous episodes of Cenozoic erosion in southwestern North America and their relationship to surface uplift, paleoclimate, paleodrainage, and paleoaltimetry: Geosphere, v. 8, no. 6, p. 1177–1206, https://doi.org/10.1130/GES00801.1.

Cole, J.C., and Braddock, W.A., 2009, Geologic map of the Estes Park 30′ × 60′ quadrangle, north-central Colorado: U.S. Geological Survey Scientific Investigations Map 3039, scale 1:100,000.

Colman, S.M., 1985, Map showing tectonic features of late Cenozoic origin in Colorado: U.S. Geological Survey Miscellaneous Investigations Series Map I-1566, scale: 1:1,000,000.

Cooperdock, E.H.G., Ketcham, R.A., and Stockli, D.E., 2019, Resolving the effects of 2-D versus 3-D grain measurements on (U-Th)/He age data and reproducibility: Geochronology, v. 1, p. 17–41, https://doi.org/10.5194/gchron-1-17-2019.

Copeland, P., Currie, C.A., Lawton, T.F., and Murphy, M.A., 2017, Location, location, location: The variable lifespan of the Laramide orogeny: Geology, v. 45, no. 3, p. 223–226, https://doi.org/10.1130/G38810.1.

Cross, T.A., and Pilger, R.H., Jr., 1978, Tectonic controls of Late Cretaceous sedimentation, Western Interior: Nature, v. 274, p. 653–657, https://doi.org/10.1038/274653a0.

DeCelles, P.G., 2004, Late Jurassic to Eocene evolution of the Cordilleran thrust belt and foreland basin system, western U.S.A.: American Journal of Science, v. 304, p. 105–168, https://doi.org/10.2475/ajs.304.2.105.

Dickinson, W.R., Klute, M.A., Hayes, M.J., Janeke, S.U., Lundin, E.R., McKittrik, M.A., and Olivares, M.D., 1988, Paleogeographic and paleotectonic setting of Laramide sedimentary basins in the central Rocky Mountain region: Geological Society of America Bulletin, v. 100, p. 1023–1039, https://doi.org/10.1130/0016-7606(1988)100<1023:PAPSOL>2.3.CO;2.

Donelick, R.A., Roden, M.K., Mooers, J.D., Carpenter, B.S., and Miller, D.S., 1990, Etchable length reduction of induced fission tracks in apatite at room temperature (~23°C): Crystallographic orientation effects and "initial" mean lengths: Nuclear Tracks and Radiation Measurements, v. 17, p. 261–265, https://doi.org/10.1016/1359-0189(90)90044-X.

Donelick, R.A., O'Sullivan, P.B., and Ketcham, R.A., 2005, Apatite fission-track analysis: Reviews in Mineralogy and Geochemistry, v. 58, p. 49–94, https://doi.org/10.2138/rmg.2005.58.3.

Ducea, M.N., Seclaman, A.C., Murray, K.E., Jianu, D., and Schoenbohm, L.M., 2013, Mantle-drip magmatism beneath the Altiplano-Puna plateau, central Andes: Geology, v. 41, no. 8, p. 915–918, https://doi.org/10.1130/G34509.1.

Eaton, G.P., 2008, Epeirogeny in the Southern Rocky Mountains region: Evidence and origin: Geosphere, v. 4, no. 5, p. 764–784, https://doi.org/10.1130/GES00149.1.

England, P., and Molnar, P., 1990, Surface uplift, uplift of rocks, and exhumation of rocks: Geology, v. 18, no. 12, p. 1173–1177, https://doi.org/10.1130/0091-7613(1990)018<1173:SUUORA>2.3.CO;2.

Epis, R.C., and Chapin, C.E., 1974, Stratigraphic nomenclature of the Thirtynine Mile Volcanic Field, Central Colorado: U.S. Geological Survey Bulletin 1395-C, 23 p.

Epis, R.C., and Chapin, C.E., 1975, Geomorphic and tectonic implication of the post-Laramide, late Eocene erosion surface in the southern Rocky Mountains, *in* Curtis, B.F., ed., Cenozoic History of the Southern Rocky Mountains: Geological Society of America Memoir 144, p. 45–74, https://doi.org/10.1130/MEM144-p45.

Epis, R.C., Scott, G.R., and Chapin, C.E., 1976, Cenozoic volcanic, tectonic, and geomorphic features of central Colorado: Colorado School of Mines Professional Contribution, v. 8, p. 323–338.

Epis, R.C., Wobus, R.A., and Scott, G.R., 1979, Geologic map of the Black Mountain quadrangle, Fremont and Park counties, Colorado: U.S. Geological Survey Miscellaneous Investigations Series Map I-1195, scale 1:62,500.

Evanoff, E., 1990, Early Oligocene paleovalleys in southern and central Wyoming: Evidence of high local relief on the Late Eocene unconformity: Geology, v. 18, no. 5, p. 443–446, https://doi.org/10.1130/0091-7613(1990)018<0443:EOPISA>2.3.CO;2.

Farley, K.A., 2000, Helium diffusion from apatite: General behavior as illustrated by Durango fluorapatite: Journal of Geophysical Research, v. 105, p. 2903–2914, https://doi.org/10.1029/1999JB900348.

Farmer, L.G., Glazner, A.F., and Manley, C.R., 2002, Did lithosphere delamination trigger late Cenozoic potassic volcanism in the southern Sierra Nevada, California?: Geological Society of America Bulletin, v. 114, p. 754–768, https://doi.org/10.1130/0016-7606(2002)114%3C0754:DLDTLC%3E2.0.CO;2.

Farmer, G.L., Bailley, T., and Elkins-Tanton, L.T., 2008, Mantle source volumes and the origin of the mid-Tertiary ignimbrite flare-up in the southern Rocky Mountains, western U.S.: Lithos, v. 102, no. 1–2, p. 279–294, https://doi.org/10.1016/j.lithos.2007.08.014.

Fleischer, R.L., Price, P.B., and Walker, R.M., 1975, Nuclear Tracks in Solids: Principles and Techniques: Berkeley, University of California Press, 605 p., https://doi.org/10.1525/9780520320239.

Flowers, R.M., Shuster, D.L., Wernicke, B.P., and Farley, K.A., 2007, Radiation damage control on apatite (U-Th)/He dates

from the Grand Canyon region, Colorado Plateau: Geology, v. 35, no. 5, p. 447–450, https://doi.org/10.1130/G23471A.1.
Flowers, R.M., Ketcham, R.A., Shuster, D.L., and Farley, K.A., 2009, Apatite (U-Th)/He thermochronometry using a radiation damage accumulation and annealing model: Geochimica et Cosmochimica Acta, v. 73, p. 2347–2365, https://doi.org/10.1016/j.gca.2009.01.015.
Foreman, B.Z., and Rasmussen, D.M., 2016, Provenance signals in the Piceance Creek Basin: Unroofing of the Sawatch Range and extent of the early Paleogene California River system (Colorado, U.S.A.): Journal of Sedimentary Research, v. 86, p. 1345–1358, https://doi.org/10.2110/jsr.2016.81.
Gallagher, K., 2012, Transdimensional inverse thermal history modeling for quantitative thermochronology: Journal of Geophysical Research, v. 117, https://doi.org/10.1029/2011JB008825.
Garcia, R.V., 2011, Cenozoic intrusive and exhumation history of the Elk and West Elk mountain plutons, Southwest Colorado [M.S. thesis]: Socorro, New Mexico Institute of Mining and Technology, 143 p.
Garzione, C.N., Auerbach, D.J., Jin-Sook Smith, J., Rosario, J.J., Passey, B.H., Jordan, T.E., and Eiler, J.M., 2014, Clumped isotope evidence for diachronous surface cooling of the Altiplano and pulsed surface uplift of the Central Andes: Earth and Planetary Science Letters, v. 393, p. 173–181, https://doi.org/10.1016/j.epsl.2014.02.029.
Gautheron, C., Tassan-Got, L., Barbarand, J., and Pagel, M., 2009, Effect of alpha-damage annealing on apatite (U-Th)/He thermochronology: Chemical Geology, v. 266, no. 3–4, p. 157–170, https://doi.org/10.1016/j.chemgeo.2009.06.001.
Gleadow, A.J., and Fitzgerald, P.G., 1987, Uplift history and structure of the Transantarctic Mountains: New evidence from fission track data of basement apatites in the Dry Valleys area, southern Victoria Land: Earth and Planetary Science Letters, v. 82, p. 1–14, https://doi.org/10.1016/0012-821X(87)90102-6.
Gregory, K.M., and Chase, C.G., 1992, Tectonic significance of paleobotanically estimated climate and altitude of the late Eocene erosion surface, Colorado: Geology, v. 20, no. 7, p. 581–585, https://doi.org/10.1130/0091-7613(1992)020<0581:TSOPEC>2.3.CO;2.
Gregory, K.M., and Chase, C.G., 1994, Tectonic and climatic significance of a Late Eocene, low-relief, high-level geomorphic surface, Colorado: Journal of Geophysical Research, v. 99, p. 20,141–20,160, https://doi.org/10.1029/94JB00132.
Guenthner, W.R., Reiners, P.W., Ketcham, R.A., Nasdala, L., and Giester, G., 2013, Helium diffusion in natural zircon: Radiation damage, anisotropy and the interpretation of zircon (U-Th)/He thermochronology: American Journal of Science, v. 313, p. 145–198, https://doi.org/10.2475/03.2013.01.
Hansen, S.M., Dueker, K.G., Stachnik, J.C., Aster, R.C., and Karlstrom, K.E., 2013, A rootless rockies—Support and lithospheric structure of the Colorado Rocky Mountains inferred from CREST and TA seismic data: Geochemistry, Geophysics, Geosystems, v. 14, p. 2670–2695, https://doi.org/10.1002/ggge.20143.
Hicks, J.F., Johnson, K.R., Obradovich, J.D., Miggins, D.P., and Tauxe, L., 2002, Magnetostratigraphy of Upper Cretaceous (Maastrichtian) to lower Eocene strata of the Denver Basin, Colorado: Rocky Mountain Geology, v. 38, no. 1, p. 1–27, https://doi.org/10.2113/gsrocky.38.1.1.
Hills, F.A., and Dickinson, K.A., 1982, Silver Plume Granite possible source of uranium in sandstone uranium deposits, Tallahassee Creek and High Park areas, Fremont and Teller counties, Colorado: U.S. Geological Survey Open-File Report 82-404, 23 p., https://doi.org/10.3133/ofr82404.
Hoblitt, R., and Larson, E., 1975, Paleomagnetic and geochronologic data bearing on the structural evolution of the northeastern margin of the Front Range, Colorado: Geological Society of America Bulletin, v. 86, p. 237–242, https://doi.org/10.1130/0016-7606(1975)86<237:PAGDBO>2.0.CO;2.
Houseman, G.A., and Molnar, P.B., 1997, Gravitational (Rayleigh-Taylor) instability of a layer with non-linear viscosity and convective thinning of continental lithosphere: Geophysical Journal International, v. 128, p. 125–150, https://doi.org/10.1111/j.1365-246X.1997.tb04075.x.
Humphreys, E., Hessler, E., Dueker, K., Erslev, E., Farmer, G.L., and Atwater, T., 2003, How Laramide-age hydration of North America by the Farallon slab controlled subsequent activity in the western United States: International Geology Review, v. 45, p. 575–595, https://doi.org/10.2747/0020-6814.45.7.575.
Hurford, A.J., 1990, Standardization of fission-track dating calibration, Recommendation by the Fission Track Working Group of the I.U.G.S. Subcommission on Geochronology: Chemical Geology, v. 80, p. 171–178, https://doi.org/10.1016/0168-9622(90)90025-8.
Jones, C.H., Farmer, G.L., and Unruh, J., 2004, Tectonics of Pliocene removal of lithosphere of the Sierra Nevada, California: Geological Society of America Bulletin, v. 116, p. 1408–1422, https://doi.org/10.1130/B25397.1.
Jones, C.H., Farmer, G.L., Sageman, B., and Zhong, S., 2011, Hydrodynamic mechanism for the Laramide orogeny: Geosphere, v. 7, no. 1, p. 183–201, https://doi.org/10.1130/GES00575.1.
Jones, C.H., Mahan, K.H., Butcher, L.A., Levandowski, W.B., and Farmer, G.L., 2015, Continental uplift through crustal hydration: Geology, v. 43, no. 4, p. 355–358, https://doi.org/10.1130/G36509.1.
Kainz, S., Abbott, L., Flowers, R., and Metcalf, J., 2021, Effect of rock strength on the documentation of an exhumation event using low temperature thermochronology: The south-central Colorado example: EGU General Assembly 2021, online, 19–30 April 2021, Abstract EGU21-13071, https://doi.org/10.5194/egusphere-egu21-13071.
Karlstrom, K.E., Coblentz, D., Dueker, K., Ouimet, W., Kirby, E., Van Wijk, J., Schmandt, B., Kelley, S., Lazear, G., Crossey, L.J., Crow, R., Aslan, A., Darling, A., Aster, R., MacCarthy, J., Hansen, S.M., Stachnik, J., Stockli, D.F., Garcia, R.V., Hoffman, M., McKeon, R., Feldman, J., Heizler, M., and Donahue, M.S., and the CREST Working Group, 2012, Mantle-driven dynamic uplift of the Rocky Mountains and Colorado Plateau and its surface response: Toward a unified hypothesis: Lithosphere, v. 4, no. 1, p. 3–22, https://doi.org/10.1130/L150.1.
Kay, R.W., and Kay, S.M., 1993, Delamination and delamination magmatism: Tectonophysics, v. 219, p. 177–189, https://doi.org/10.1016/0040-1951(93)90295-U.
Kelley, S.A., and Chapin, C.E., 2004, Denudation history and internal structure of the Front Range and Wet Mountains, Colorado, based on apatite-fission-track thermochronology, *in* Cather, S.M., et al., eds., Tectonics, Geochronology, and Volcanism in the southern Rocky Mountains and Rio Grande Rift: New Mexico Bureau of Geology and Mineral Resources Bulletin, v. 160, p. 41–68.
Keller, S.M., and Morgan, M.L., 2016, Overview of the Eocene Castle Rock Conglomerate, east-central Colorado: Remapping the fluvial system, and implications for the history of the Colorado Piedmont and Front Range, *in* Keller, S.M., and Morgan, M.L., eds., Unfolding the Geology of the West: Geological Society of America Field Guide 44, p. 125–141, https://doi.org/10.1130/2016.0044(05).
Kellogg, K.S., 1999, Neogene basins of the northern Rio Grande rift: Partitioning and asymmetry inherited from Laramide and older uplifts: Tectonophysics, v. 305, p. 141–152, https://doi.org/10.1016/S0040-1951(99)00013-X.
Ketcham, R.A., 2005, Forward and inverse modeling of low-temperature thermochronometry data, *in* Reiners, P.W., and Ehlers, T.A., eds., Thermochronology: Reviews in Mineralogy & Geochemistry, v. 58, p. 275–314, https://doi.org/10.1515/9781501509575-013.
Ketcham, R.A., Carter, A., Donelick, R.A., Barbarand, J., and Hurford, A.J., 2007, Improved modeling of fission-track annealing in apatite: The American Mineralogist, v. 92, p. 799–810, https://doi.org/10.2138/am.2007.2281.
Ketcham, R.A., Gautheron, C., and Tassan-Got, L., 2011, Accounting for long alpha-particle stopping distances in (U-Th-Sm)/He geochronology: Refinement of the baseline case: Geochimica et Cosmochimica Acta, v. 75, p. 7779–7791, https://doi.org/10.1016/j.gca.2011.10.011.
Koch, A.J., Coleman, D.S., and Sutter, A.M., 2018, Provenance of the upper Eocene Castle Rock Conglomerate, south Denver Basin, Colorado, U.S.A.: Rocky Mountain Geology, v. 53, p. 29–43, https://doi.org/10.24872/rmgjournal.53.1.29.
Landman, R.L., 2016, Thermochronologic investigations of Cenozoic unroofing and surface uplift in the southern Rocky Mountains and Great Plains [Ph.D. thesis]: Boulder, University of Colorado, 274 p.
Landman, R.L., and Flowers, R.M., 2013, (U-Th)/He thermochronologic constraints on the evolution of the northern Rio Grande rift, Gore Range, Colorado and implications for rift propagation models: Geosphere, v. 9, no. 1, p. 170–187, https://doi.org/10.1130/GES00826.1.
Lee, D.K., and Grand, S.P., 1996, Upper mantle shear structure beneath the Colorado Rocky Mountains: Journal of Geophysical Research, v. 101, p. 22,233–22,244, https://doi.org/10.1029/96JB01502.
Leonard, E.M., and Langford, R.P., 1994, Post-Laramide deformation along the eastern margin of the Colorado Front Range—A case against significant faulting: The Mountain Geologist, v. 31, p. 45–52.
Levander, A., and Miller, M.S., 2012, Evolutionary aspects of the lithosphere discontinuity structure in the western U.S.: Geochemistry, Geophysics, Geosystems, v. 13, Q0AK07, https://doi.org/10.1029/2012GC004056.
Lipman, P.W., 2021, Raising the West: Mid-Cenozoic Colorado-plano related to subvolcanic batholith assembly in the Southern Rocky Mountains (USA)?: Geology, v. 49, no. 9, p. 1107–1111, https://doi.org/10.1130/G48963.1.
Lord, A.B.H., McGregor, H., Roden, M.F., Salters, V.J.M., Sarafian, A., and Leahy, R., 2016, Petrogenesis of coeval sodic and potassic alkaline magmas at Spanish Peaks, Colorado: Magmatism related to the opening of the Rio Grande rift: Geochimica et Cosmochimica Acta, v. 185, p. 453–476, https://doi.org/10.1016/j.gca.2016.04.019.
MacGinitie, H.D., 1953, Fossil plants of the Florissant beds, Colorado: Contributions to Paleontology 40: Carnegie Institution of Washington Publication 599, 198 p.

McIntosh, W.C., and Chapin, C.E., 2004, Geochronology of the central Colorado volcanic field: New Mexico Bureau of Geology and Mineral Resources Bulletin, v. 160, p. 205–237.
McMillan, M.E., Angevine, C.L., and Heller, P.L., 2002, Postdepositional tilt of the Miocene-Pliocene Ogallala Group on the western Great Plains: Evidence of late Cenozoic uplift of the Rocky Mountains: Geology, v. 30, no. 1, p. 63–66, https://doi.org/10.1130/0091-7613(2002)030<0063:PTOTMP>2.0.CO;2.
Meyer, H.W., 1992, Lapse rates and other variables applied to estimating paleoaltitudes from fossil floras: Palaeogeography, Palaeoclimatology, Palaeoecology, v. 99, p. 71–99, https://doi.org/10.1016/0031-0182(92)90008-S.
Molnar, P., 2004, Late Cenozoic increase in accumulation rates of terrestrial sediment: How might climate change have affected erosion rates?: Annual Review of Earth and Planetary Sciences, v. 32, p. 67–89, https://doi.org/10.1146/annurev.earth.32.091003.143456.
Molnar, P., and England, P., 1990, Late Cenozoic uplift of mountain ranges and global climate change: Chicken or egg?: Nature, v. 346, p. 29–34, https://doi.org/10.1038/346029a0.
Moucha, R., Forte, A.M., Rowley, D.B., Mitrovica, J.X., Simmons, N.A., and Grand, S.P., 2008, Mantle convection and the recent evolution of the Colorado Plateau and the Rio Grande Rift valley: Geology, v. 36, no. 6, p. 439–442, https://doi.org/10.1130/G24577A.1.
Obradovich, J.D., Mutschler, F.E., and Bryant, B., 1969, Potassium-argon ages bearing on the igneous and tectonic history of the Elk Mountains and vicinity, Colorado—A preliminary report: Geological Society of America Bulletin, v. 80, p. 1749–1756, https://doi.org/10.1130/0016-7606(1969)80[1749:PABOTI]2.0.CO;2.
Pelletier, J., 2009, The impact of snowmelt on the late Cenozoic landscape of the southern Rocky Mountains, USA: GSA Today, v. 19, no. 7, p. 4–10, https://doi.org/10.1130/GSATG44A.1.
Raynolds, R.G., 1997, Synorogenic and post-orogenic strata in the central Front Range, Colorado, *in* Bolyard, D.W., and Sonnenberg, S.A., eds., Geologic History of the Colorado Front Range, 1997 RMS-AAPG Field Trip #7: Denver, Rocky Mountain Association of Geologists, p. 43–48.
Reiners, P.W., and Farley, K.A., 1999, Helium diffusion and (U-Th)/He thermochronometry of titanite: Geochimica et Cosmochimica Acta, v. 63, p. 3845–3859, https://doi.org/10.1016/S0016-7037(99)00170-2.
Reiners, P.W., and Farley, K.A., 2001, Influence of crystal size on apatite (U-Th)/He thermochronology: An example from the Bighorn Mountains, Wyoming: Earth and Planetary Science Letters, v. 188, p. 413–420, https://doi.org/10.1016/S0012-821X(01)00341-7.
Reiners, P.W., Farley, K.A., and Hickes, H.J., 2002, He diffusion and (U-Th)/He thermochronometry of zircon: Initial results from Fish Canyon Tuff and Gold Butte: Tectonophysics, v. 349, p. 297–308, https://doi.org/10.1016/S0040-1951(02)00058-6.
Ricketts, J.W., Kelley, S.A., Karlstrom, K.E., Schmandt, B., Donahue, M.S., and van Wijk, J., 2016, Synchronous opening of the Rio Grande rift along its entire length at 25–10 Ma supported by apatite (U-Th)/He and fission-track thermochronology, and evaluation of possible driving mechanisms: Geological Society of America Bulletin, v. 128, p. 397–424, https://doi.org/10.1130/B31223.1.
Rosenberg, R., Kirby, E., Aslan, A., Karlstrom, K.E., Heizler, M., and Ouimet, W., 2014, Late Miocene erosion and evolution of topography along the western slope of the Colorado Rockies: Geosphere, v. 10, no. 4, p. 641–663, https://doi.org/10.1130/GES00989.1.
Sahagian, D., Proussevitch, A., and Carlson, W., 2002, Timing of Colorado Plateau uplift: Initial constraints from vesicular basalt-derived paleoelevations: Geology, v. 30, p. 807–810, https://doi.org/10.1130/0091-7613(2002)030<0807:TOCPUI>2.0.CO;2.
Schmandt, B., and Humphreys, E., 2010, Complex subduction and small-scale convection revealed by body-wave tomography of the western United States upper mantle: Earth and Planetary Science Letters, v. 297, p. 435–445, https://doi.org/10.1016/j.epsl.2010.06.047.
Scott, G.R., 1975, Cenozoic surfaces and deposits in the Southern Rocky Mountains, *in* Curtis, B.F., ed., Cenozoic History of the Southern Rocky Mountains: Geological Society of America Memoir 144, p. 227–248, https://doi.org/10.1130/MEM144-p227.
Scott, G.R., and Taylor, R.B., 1986, Map showing Late Eocene erosion surface, Oligocene–Miocene paleovalleys, and Tertiary deposits in the Pueblo, Denver, and Greeley 1° × 2° quadrangles, Colorado: U.S. Geological Survey Miscellaneous Investigations Series Map I-1626, scale 1:250,000.
Sheehan, A.F., Abers, G.A., Jones, C.H., and Lerner-Lam, A., 1995, Crustal thickness variations across the Colorado Rocky Mountains from teleseismic receiver functions: Journal of Geophysical Research, v. 100, p. 20,391–20,404, https://doi.org/10.1029/95JB01966.
Shuster, D.L., Flowers, R.M., and Farley, K.A., 2006, The influence of natural radiation damage on helium diffusion kinetics in apatite: Earth and Planetary Science Letters, v. 249, p. 148–161, https://doi.org/10.1016/j.epsl.2006.07.028.
Spencer, J.E., 1996, Uplift of the Colorado Plateau due to lithosphere attenuation during Laramide low-angle subduction: Journal of Geophysical Research, v. 101, p. 13,595–13,609, https://doi.org/10.1029/96JB00818.
Stanley, J.R., Flowers, R.M., and Bell, D.R., 2013, Kimberlite (U-Th)/He dating links surface erosion with lithospheric heating, thinning and metasomatism in the southern African Plateau: Geology, v. 41, p. 1243–1246, https://doi.org/10.1130/G34797.1.
Stanley, J.R., Flowers, R.M., and Bell, D.R., 2015, Erosion patterns and mantle sources of topographic change across the southern African Plateau derived from the shallow and deep records of kimberlites: Geochemistry, Geophysics, Geosystems, v. 16, p. 3235–3256, https://doi.org/10.1002/2015GC005969.
Stockli, D.F., and Farley, K.A., 2004, Empirical constraints on the titanite (U-Th)/He partial retention zone from the KTB drill hole: Chemical Geology, v. 207, p. 223–236, https://doi.org/10.1016/j.chemgeo.2004.03.002.
Thorson, J.P., 2011, Geology of Upper Cretaceous, Paleocene and Eocene strata in the southwestern Denver Basin, Colorado: Golden, Colorado Geological Survey, OF-11-02, 53 p.
Trimble, D.E., 1980, Cenozoic tectonic history of the Great Plains contrasted with that of the Southern Rocky Mountains: A synthesis: The Mountain Geologist, v. 17, p. 59–69.
Tweto, O., 1975, Laramide (Late Cretaceous–Early Tertiary) Orogeny in the Southern Rocky Mountains, *in* Curtis, B.F., ed., Cenozoic History of the Southern Rocky Mountains: Geological Society of America Memoir 144, p. 1–44, https://doi.org/10.1130/MEM144-p1.
Tweto, O., 1979, Geologic map of Colorado: U.S. Geological Survey, scale 1:500,000.
Tweto, O., 1987, Rock units of the Precambrian basement in Colorado: U.S. Geological Survey Professional Paper 1321-A, 54 p., https://doi.org/10.3133/pp1321A.
van Wijk, J., Koning, D., Axen, G., Coblenz, D., Gragg, E., and Sion, B., 2018, Tectonic subsidence, geoid analysis, and the Miocene–Pliocene unconformity in the Rio Grande rift, southwestern United States: Implications for mantle upwelling as a driving force for rift opening: Geosphere, v. 14, p. 684–709, https://doi.org/10.1130/GES01522.1.
Wallace, C.A., and Lawson, A.D., 2008, Geologic map of the Cameron Mountain quadrangle, Chaffee, Fremont, and Park counties, Colorado: Colorado Geological Survey Open-File Report 08-12, scale 1:24,000.
Wallace, C.A., Cappa, J.A., and Lawson, A.D., 1997, Geologic map of the Salida East quadrangle, Fremont County, Colorado: Colorado Geological Survey Open-File Report 97-6, scale 1:24,000.
Wallace, C.A., Cappa, J.A., and Lawson, A.D., 1999, Geologic map of the Gribbles Park quadrangle, Park and Fremont counties, Colorado: Colorado Geological Survey Open-File Report 99-3, scale 1:24,000.
Wallace, C.A., Apeland, A.D., and Cappa, J.A., 2000, Geologic map of the Jack Hall Mountain quadrangle, Fremont County, Colorado: Colorado Geological Survey Open-File Report 00-1, scale 1:24,000.
Wobus, R.A., and Epis, R.C., 1978, Geologic map of the Florissant quadrangle, Park and Teller counties, Colorado: U.S. Geological Survey Miscellaneous Investigations Series Map I-1044, scale 1:62,500.
Wobus, R.A., Epis, R.C., and Scott, G.R., 1979, Geologic map of the Cover Mountain quadrangle, Fremont, Park, and Teller counties, Colorado: U.S. Geological Survey Miscellaneous Investigations Series Map I-1179, scale 1:62500.
Wofford, M.K.Y., 1986, Skarn formation adjacent to the Whitehorn stock, Chaffee County, Colorado [M.S. thesis]: Lubbock, Texas Tech University, 72 p.
Wolfe, J.A., Forest, C.E., and Molnar, P., 1998, Paleobotanical evidence of Eocene and Oligocene paleoaltitudes in midlatitude western North America: Geological Society of America Bulletin, v. 110, p. 664–678, https://doi.org/10.1130/0016-7606(1998)110<0664:PEOEAO>2.3.CO;2.
Wrucke, C.T., 1974, The Whitehorn Granodiorite of the Arkansas Valley in central Colorado: U.S. Geological Survey Bulletin 1394-H, 7 p.
Wrucke, C.T., and Dings, M.G., 1979, Geologic map of the Cameron Mountain quadrangle, Colorado: U.S. Geological Survey Open-File Report 79-660, map scale 1:62500.
Ye, H., Royden, L., Burchfiel, C., and Schuepbach, M., 1996, Late Paleozoic Deformation of Interior North America: The Greater Ancestral Rocky Mountains: American Association of Petroleum Geologists Bulletin, v. 80, p. 1397–1432.
Zaborac-Reed, S.J., and Leopold, E.B., 2016, Determining the paleoclimate and elevation of the late Eocene Florissant flora: Support from the coexistence approach: Canadian Journal of Earth Sciences, v. 53, p. 565–573, https://doi.org/10.1139/cjes-2015-0165.
Zachos, J., Pagani, M., Sloan, L., Thomas, E., and Billups, K., 2001, Trends, rhythms, and aberrations in global climate 65 Ma to present: Science, v. 292, p. 686–693, https://doi.org/10.1126/science.1059412.